MONAZITE (U-TH-PB) DATING OF POLYPHASE TECTONOMETAMORPHISM IN THE GOVERNMENT POINT AND CUNARD FORMATIONS, SW NOVA SCOTIA

Daniel G. Pfeiffer

Submitted in partial fulfillment of the requirements
for the degree of Bachelor of Science, Honours
Department of Earth Science
Dalhousie University, Halifax, Nova Scotia
April 2013

Distribution License

DalSpace requires agreement to this non-exclusive distribution license before your item can appear on DalSpace.

NON-EXCLUSIVE DISTRIBUTION LICENSE

You (the author(s) or copyright owner) grant to Dalhousie University the non-exclusive right to reproduce and distribute your submission worldwide in any medium.

You agree that Dalhousie University may, without changing the content, reformat the submission for the purpose of preservation.

You also agree that Dalhousie University may keep more than one copy of this submission for purposes of security, back-up and preservation.

You agree that the submission is your original work, and that you have the right to grant the rights contained in this license. You also agree that your submission does not, to the best of your knowledge, infringe upon anyone's copyright.

If the submission contains material for which you do not hold copyright, you agree that you have obtained the unrestricted permission of the copyright owner to grant Dalhousie University the rights required by this license, and that such third-party owned material is clearly identified and acknowledged within the text or content of the submission.

If the submission is based upon work that has been sponsored or supported by an agency or organization other than Dalhousie University, you assert that you have fulfilled any right of review or other obligations required by such contract or agreement.

Dalhousie University will clearly identify your name(s) as the author(s) or owner(s) of the submission, and will not make any alteration to the content of the files that you have submitted.

If you have questions regarding this license please contact the repository manager at dalspace@dal.ca.

Grant the distribution license by signing and dating below.

_____ _____

Name of signatory Date

DALHOUSIE UNIVERSITY
Inspiring Minds

Department of Earth Sciences
Halifax, Nova Scotia
Canada B3H 4R2
(902) 494-2358
FAX (902) 494-6889

DATE: April 30th, 2013

AUTHOR: Daniel Pfeiffer

TITLE: Monazite (U-Th-Pb) dating of polyphase tectono-metamorphism in the Government Point and Cunard formations, SW Nova Scotia

Degree: BSc Honours Convocation: May Year: 2013

Monazite (U-Th-Pb) dating of polyphase tectono-metamorphism in the Government Point and Cunard formations, SW Nova Scotia

Daniel G. Pfeiffer
Department of Earth Sciences, Dalhousie University, Halifax, NS, B3H 4J1 dn237548@dal.ca

The ages of monazite crystals from metapelitic rock samples from the southwest Nova Scotia have been examined using in-situ dating methods. The rocks are from the Government Point and Cunard formations of the Goldenville Group and Halifax Group respectively which are characterized as andalusite- and staurolite-bearing schists. The protoliths are thought to be turbiditic sediments deposited off the passive margin of Gondwana and subsequently deformed during the assembly of Pangaea. The peak equilibrium mineral assemblage suggests a lower to medium amphibolite facies under conditions of approximately 550-600°C and 2.5 kb. These metasedimentary rocks contain an inclusion-rich staurolite poikiloblastic fabric that has been overprinted by inclusion-poor staurolite porphyroblasts. These textures are interpreted as evidence of polyphase metamorphism associated with the lower- to mid-Devonian Neoacadian orogeny.

Monazite, a LREE phosphate, is widely used as a chronometer due to its unique chemical signature and high Th and U contents. Transmitted light microscopy textural characterization and electron microprobe chemical microanalysis has been performed on samples from the region to constrain the timing of the distinct tectonometamorphic events recorded by these samples. Compositional mapping of monazite grains in these rocks has identified concentric zonation defined by Y concentration resulting from the breakdown of garnet, staurolite and xenotime under prograde and retrograde metamorphic conditions. This suggests multiple stages of metamorphism preserved within monazite.

Chronology of the individual metamorphic monazite grains yielded an age range of 370±6 which represent the post-deformation contact metamorphism associated with the Acadian orogeny that affected the rocks of southwest Nova Scotia. Analysis has also determined a significant portion of the monazite grains are detrital (ages 1000-450 Ma) with partial resetting corresponding to post-depositional deformation and metamorphism.

Table of Contents

List of Figures

List of Tables

Acknowledgements

I would like to express my sincere thanks to my supervisor, Dr. Richard Cox, for his guidance, support and patience throughout the completion of this project. Richard's knowledge of geochemical relationships and mineralogy was invaluable during analysis and interpretation. I would also like to extend thanks to Dr. Becky Jamieson for the generous use of her thin and polished sections as well as her direction in identifying and interpreting metamorphic textures.

In addition to Richard and Becky, I need to thank Dan MacDonald for his expertise and assistance while performing microprobe analysis and Mike Young for his critiques and suggestions. As well, I own many thanks to Dr. Martin Gibling for his careful revisions and continued encouragement which provided significant improvements throughout every stage of my research.

Finally, a special thanks needs to be extended to the members of the 2013 Honours class whose support and camaraderie were integral to the completion of this project.

1.0 Introduction

1.1 Statement of Problem

The metasedimentary rocks of the Meguma Supergroup in southwestern Nova Scotia have undergone polyphase metamorphism and deformation associated with the lower to mid Devonian Neoacadian orogeny. These metasediments have preserved mineral assemblages and textures that record pressure and temperature (P-T) conditions achieved during the multiple stages of this orogenic event. These assemblages contain accessory monazite and xenotime grains which, when analyzed chemically, can yield information related to the age of the individual deformation events. The objective of this study is to interpret the chemical variations that exist within individual monazite grains to determine a numerical age for the deformation events that have affected the metasedimentary rocks of southwestern Nova Scotia.

1.2 Regional Geology

The Halifax and Goldenville groups of the Meguma Terrane are present in outcrop throughout southwestern Nova Scotia and are characterised by thick metamorphosed turbiditic sequences deposited along the margin of Gondwana during the Upper Proterozoic-Lower Ordovician (White, 2010). The Goldenville Group is distinguished from the overlying Halifax Group based on grain size with the Halifax representing basinal deposition of black slate and siltstones whereas the Goldenville has more source-proximal properties and is characterised by sandstone units (Schenk, 1997). The youngest age measured for the Goldenville Group is 544±18 Ma through use of detrital zircon while fossil fragments preserved in the overlying Halifax Group indicates an Early Ordovician deposition age (Waldron et al., 2009; White, 2010). These turbidite deposits were subjected to strong deformation and intruded by numerous Mid to

Upper Devonian, peraluminous-granitic plutons during the accretion and orogenesis that occurred as a result of collision that formed the supercontinent of Pangaea (White, 2010). The Shelburne and Barrington Passage Plutons, which are located proximal to the study area, are compositionally described as monzogranitic and granodioritic based on biotite content (Rogers and Barr, 1988). This pluton was dated using U-Pb ratios derived from concordant monazite and zircon grains and provides an intrusion age of 372±2Ma (Keppie and Krogh, 1999).

Deformation and metamorphism during this collision produced metamorphic assemblages within these sedimentary rock units. There have been projects undertaken to constrain the timing associated with deformation utilizing samples from southern Nova Scotia. These tests have specifically utilized K–Ar and $^{40}Ar/^{39}Ar$ dating of muscovite which has a closure temperature of approximately 430-380°C as well as U-Pb dating of zircon and monazite (Winter, 2010). The results of these tests yielded age ranges which possess a dichotomous relationship. K–Ar whole-rock analysis determined the age for a suite of sampled micas at 600-550 Ma which is significantly older than the accepted age range of the Devonian Acadian orogeny. The other age value identified by this analysis ranged from 395-388 Ma (Hicks et al., 1999). The interpretation of these data is that the older range represents detrital muscovite which was not reset by the regional metamorphism while the younger age range micas were the product of the low-grade regional metamorphism (Hicks et al., 1999). Similar results were produced based on analysis of the zircon and monazite grains with a reported Acadian Orogeny deformation age of 378±1 Ma (Greenough et al., 1999). This analysis was performed on basement xenoliths hosted in the Weekend dyke swarm on the eastern shore of Nova Scotia.

This study will focus on samples representative of the Government Point Formation of the Goldenville Group and the Cunard Formation of the Halifax Group as they appear in outcrop

in southwestern Nova Scotia. The Government Point Formation in the region of Jordan Falls is described as an andalusite-staurolite-cordierite granofels while the Cunard Formation is described as an andalusite schist due to its large proportion of the aluminum silicate (White, 1984; White, 2010). Rocks in the area are of medium metamorphic grade/amphibolite facies. Poikiloblasts of staurolite, garnet, andalusite, cordierite and biotite are common within these rocks (Schenk, 1997). Two generations of staurolite poikiloblasts are present within the rocks of this region. Staurolite with numerous inclusions of quartz and graphite are interpreted to have crystallised from the metapelitic matrix which would represent the first deformation event (Waldron et al, 2009). Staurolite poikiloblasts with no inclusions are also present and appear to have grown at the expense of biotite (White, 1984). These inclusion-poor staurolites are interpreted to have overprinted the earlier fabric and represent and second or greater order deformation event.

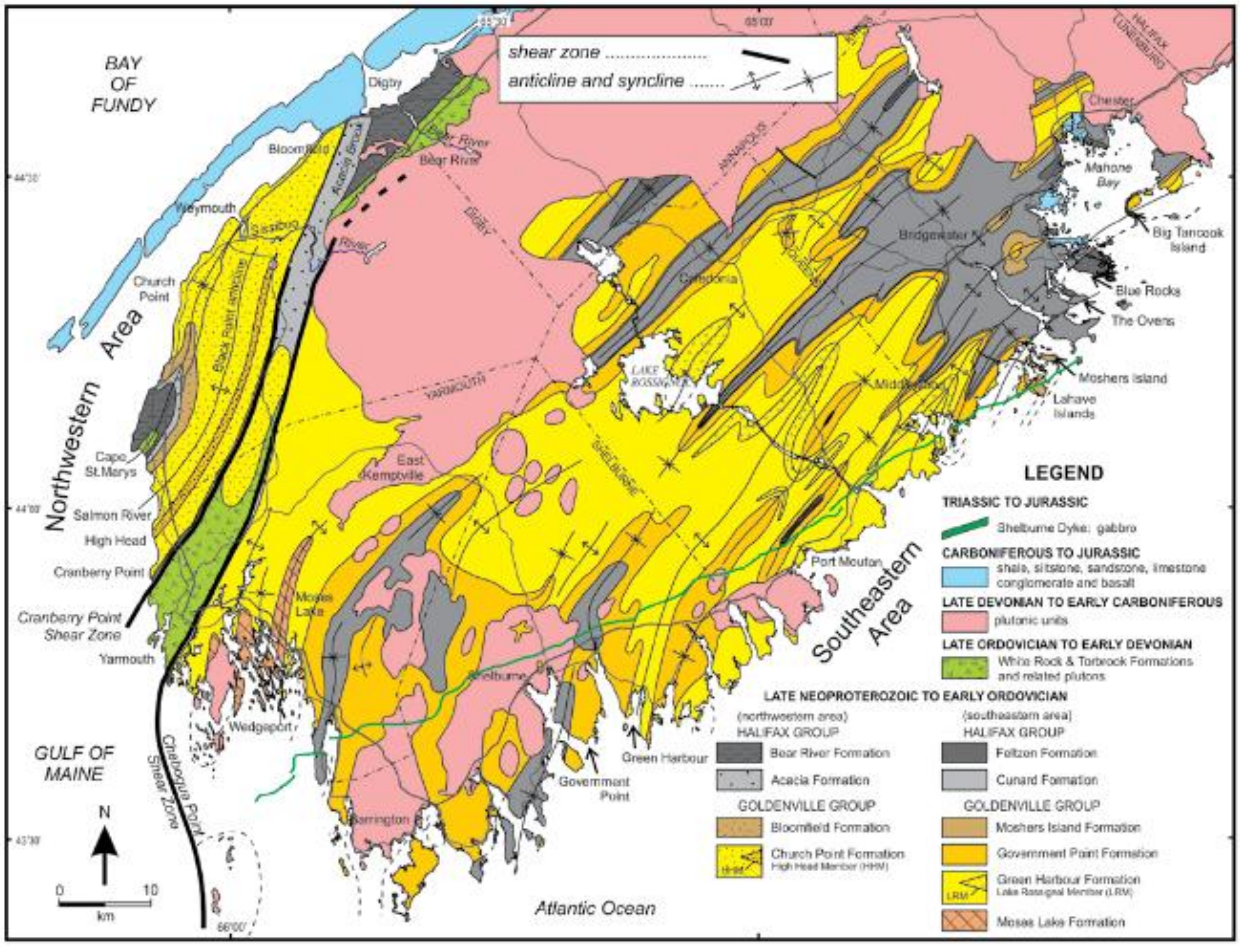

Fig.1: Geological map of southern Nova Scotia (White, 2010).

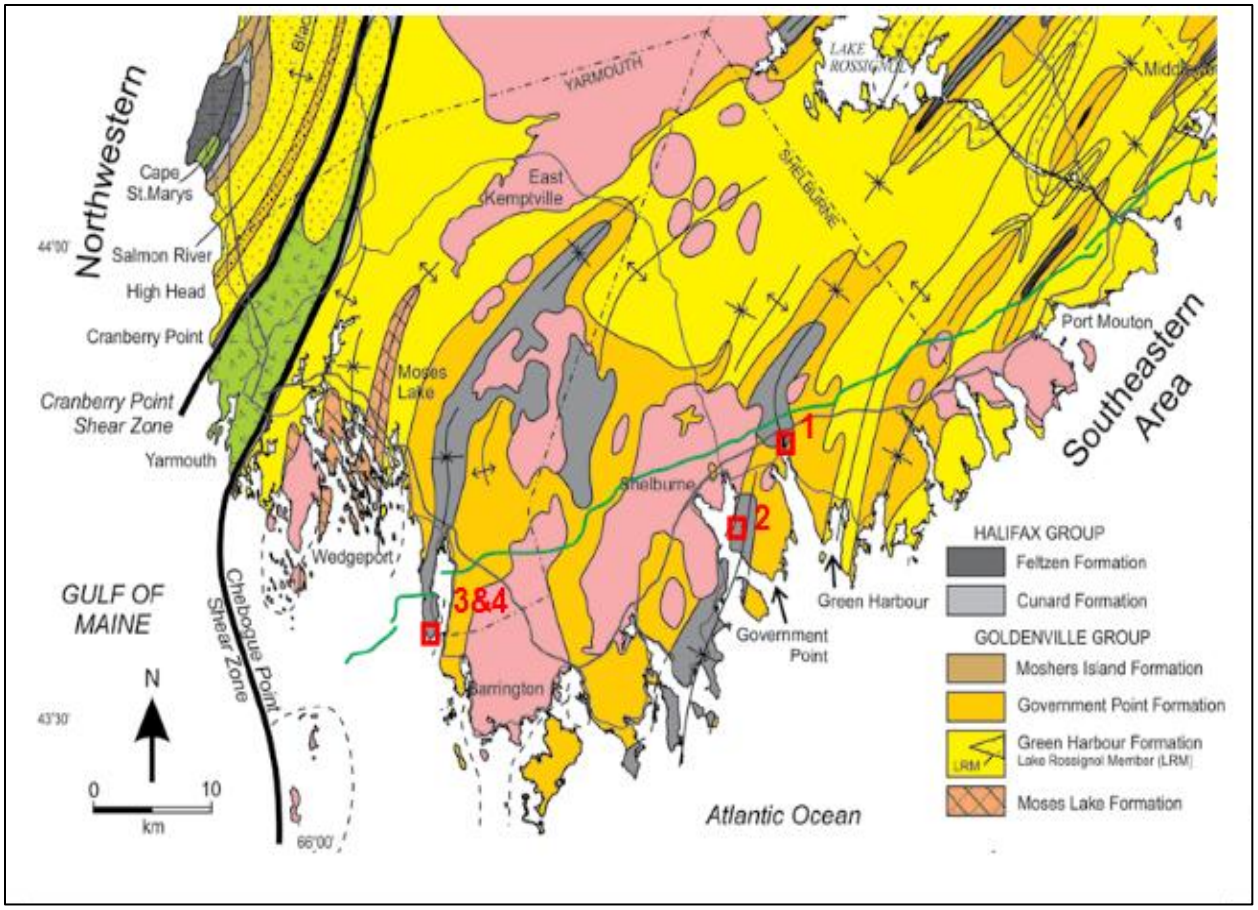

Fig.2: Geology of southwest Nova Scotia. Sample locations annotated and correspond as follows; 1=SWM6, 2=SWM8, 3=SWM13 & 4=SWM14 (Modified from White, 2010).

1.3 Properties of Monazite

Monazite [Ce,La,Nd,Th,Y)PO_4] is a light rare earth element (LREE)-bearing phosphate mineral that occurs as an accessory mineral in igneous and metamorphic rocks (Williams, 2002). Monazite in metamorphic rocks is produced primarily as a result of the breakdown of earlier phosphates (eg. Apatite, Xenotime) and garnet, the principal REE-bearing major silicate, based on the stability parameters of temperature and pressure within the sample (Winter, 2010). The composition of monazite depends on the composition, mineralogy, reaction history and deformation conditions experienced by the host rock which are in turn represented in the mineral. Compositionally, monazite is similar to another REE-bearing phosphate, xenotime

[HREE(PO4)] but these minerals can be differentiated on the basis of crystal structure with monazite coordinated by a nine-oxygen polyhedral structure and xenotime by a dodecahedron cation-bonded structure (Williams, 2007) Monazite exists in a solid solution ternary system defined by the end-member classifications of $2REEPO_4$-$CaTh(PO_4)_2$-$2ThSiO_4$ (Linthout, 2007). The mineral names as applied to the members of the ternary system are summarized in **Table 1**.

Mineral Name	Formula
Monazite	
Monazite-(Ce)	$(Ce,La,Nd,Th)PO_4$
Monazite-(La)	$(La,Ce,Nd)PO_4$
Monazite-(Nd)	$(Nd,La,Ce)PO_4$
Monazite-(Sm)	$(Sm,Gd,Ce,Th,Ca)PO_4$
Cheralite	$(LREE,Th,U,Ca,Pb)(P,Si)O_4$
Huttonite	$ThSiO_4$

Table 1: Classification of monazite species by end-member differentiation (Linthout, 2007).

1.4 Monazite-Forming Reactions

Monazite is rarely observed in low-grade pelitic metamorphic rocks but is relatively abundant in samples of amphibolite-grade and higher (Williams, 2007). This has prompted investigations into monazite-forming reactions. The reactions that contribute to the formation of monazite are generally poorly understood but it is accepted that during prograde metamorphism, the breakdown of REE-bearing minerals is crucial for the production of monazite. The most cited monazite forming reaction involves the stability ranges for allanite $[(Ca,Ree)_2(Al,Fe,Mg)_3Si_3O_{12}(OH)]$ and monazite. It has been determined that the breakdown of allanite to produce monazite occurs at approximately 550°C or above the garnet grade Barrovian zone (Williams, 2007). There have also been studies into the breakdown of titanite which would also act as a REE source for monazite crystallization (Pan, 1997). The proposed reaction is as follows:

$$Tnt + (CO_2)^{2-} + (PO_4)^{3-} + F^- + (OH)^-$$
$$\rightarrow Mnz + Qtz + Cal + Rt + Ep + Bastnäsite + Chl$$

Along with these reactions, it has been proposed that other primary minerals which could serve as a REE source for monazite are apatite [$Ca_5(PO_4)_3(F,Cl,OH)$] and garnet [$(Mg,Fe,Mn,Ca)_3(Al,Fe)_2(SiO_4)_3$] (Spear, 2002). Garnet, a REE-bearing silicate, has been identified as a source for zircon in metamorphic rocks and this reactive property has been applied to the formation of monazite through similar processes. It has been determined through previous investigation that monazite is not present within the garnet zone but can be observed in equilibrium with staurolite. Because of this it has been suggested that monazite is an accessory mineral produced by the progade staurolite-in reaction involving the breakdown of garnet (Kohn, 2004). The staurolite in reaction presented by Kohn and Malloy (2004) is as follows:

$$Grt + Ms + Chl \rightarrow Bt + St + Plag + Qtz + H_2O$$

Apatite, as a REE-bearing phosphate mineral, seems a likely candidate as a monazite producing reactant. It would also appear likely that the combination of these reactive minerals beyond their respective stability fields would form monazite. This has been quantified by the following reaction (as per Bingin and van Breemen, 1998):

$$3Tnt/Hbl + 3Aln + 2Ap + 6Qtz \rightarrow 6Mnz + 2Ap + 6Plag$$

These monazite-forming reactions are the means by which successive tectono-metamorphic events are imprinted upon individual grains of monazite. As these reactions involve minerals of highly variable compositions, the different events impart a unique compositional profile on the monazite grains producing the discrete compositional domains that can be chemically detected and form the basis for this research.

1.5 Detrital Monazite

The properties of monazite which contribute to its viability for geochronologic analysis also provide a means for the preservation of detrital grains in metamorphosed sediments. Detrital monazite is a valuable tool for provenance studies in sedimentary basins as monazite records lower temperature events than zircon, a highly resistant igneous mineral which is often preserved in sedimentary basins. As mentioned above, monazite grows as the result of deformation, but can also form in intrusive granitic systems or as a hydrothermal alteration product at temperatures above 300°C (Triantafyllidis at al., 2010). The eastern portion of the North American continent is banded by extinct orogenic belts which, during formation, would have formed monazites in response to collisional magmatism and metamorphic deformation. As these orogenic belts developed and were subsequently eroded, the resistant monazite grains were transported and deposited as passive margin sediments. These passive margin turbidite deposits were then subjected to later stage deformation as they contributed to the formation of younger orogenies (Fig.3). In the case of southwest Nova Scotia, the Grenville Orogeny (1200-950 Ma) and various Neoproterozoic (eg. Caledonian) orogenies (620-450 Ma) would likely have contributed sediment to the passive margin deposition of the Goldenville and Halifax groups (Waldron et al., 2009). Analysis of off-shore collected, Meguma sourced, detrital monazites by Triantafyllidis at al. (2010) yielded age populations ranging from as young as 200 Ma to older than 2200 Ma indicating numerous sources of detrital monazites. As post-depositon deformation affected the detrital monazites, diffusions rates within the grain, which would be negligible under standard diagenetic conditions, can increased in response to the increased temperature. At higher temperatures, such as those experienced during regional metamorphism, this diffusion will cause

partial resetting of the chemical ratios leading to an averaging effect between the detrital age and the age of the subsequent deformation.

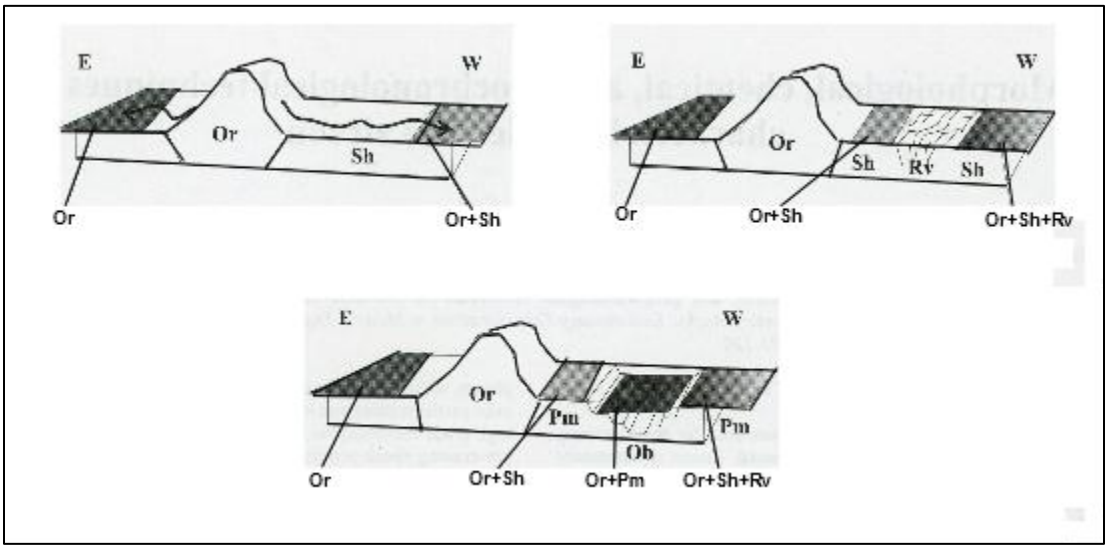

Fig.3: Distribution of detrital grains in an evolving continental setting. Abbreviations: Or-orogenic belt, Sh-shield, Rm-rift margin, Rv-rift volcanics, Pm-passive margin and Ob-oceanic basin (Cox, 2003).

1.6 U-Th-Pb Isotope Dating

Monazite is nearly universally present in pelitic rocks of the amphibolite facies and above and also typically contains significant concentrations of U, Th and Y with trace amounts of Pb, considered to be purely radiogenic, which makes it a suitable candidate for U-Pb isotope dating of metamorphic rock samples (Williams, 2007). Through analysis, the proportions of U, Th and Pb can be determined and these concentrations can be used to calculate an age of the sample using the following formula:

$$Pb = \left[\frac{Th}{232}\left(e^{\lambda 232t} - 1\right)\right] 208 + \left[\frac{U}{238} 0.9928\left(e^{\lambda 238t} - 1\right)\right] 206$$

$$+ \left[\frac{U}{235} 0.0072\left(e^{\lambda 235t} - 1\right)\right] 207$$

With Pb, Th and U as the quantities of the respective elements, t being time and λ^{232}, λ^{238}, λ^{235} representing the decay constants of Th^{232}, U^{238} and U^{235}, respectively (Williams, 2007). The most direct monazite dating technique in metamorphic petrology involves the composition variation that exists between inclusions in distinct porphyroblasts and in the matrix. By measuring the abundance of these elements, monazite inclusions within porphyroblasts can be assigned age ranges that can be used to determine the age of the metamorphic event that caused the growth of the porphyroblast (Williams, 2007). Chemical analysis of samples can be performed with the use of the Electron Microprobe (EMP) and measurement of specific isotopes for isotopic dating requires the use of mass spectrometry. This dating method can be applied to the study of textural geochronology. Accuracy in dating samples using this technique requires certain criteria be meet by the mineral being tested. These criteria are (1) a variable composition must be present to provide data sourced by multiple tectono-metamorphic events, (2) Diffusion of elements within the crystal structure must be slow to non-existent to prevent leaching between compositional domains, (3) a high "blocking temperature" (the temperature at which a given mineral is no longer able to hold its chemical and isotopic signature) and (4) the mineral being used must be highly stable to prevent contamination of the sample (Winter, 2010). The properties of monazite satisfy these criteria.

Monazite develops during prograde and retrograde breakdown of other minerals. As the tectono-metamorphic conditions change, monazite grows discrete compositional domains as a result of precipitation. These chemically variable domains represent individual events which can be isotopically measured. Diffusion through the crystal structure of monazite is very slow which prevents radiogenic Pb from crossing and contaminating compositional domains. The blocking temperature of monazite is approximately 800°C which allows the integrity of the system to be

maintained under high-grade metamorphic conditions (Winter, 2010). Without this, the chemical zonation within the monazite grains would likely be reset by younger tectono-metamorphic events. The stability of monazite is such that it is able to survive a wide range of temperature and pressure conditions and will likely be preserved throughout subsequent tectono-metamorphic events as well as during the processes of exhumation and weathering. With these criteria met, the U,Th and Pb concentrations can be measured and a pressure-temperature-time-deformation (P-T-*t*-D) history for the sample can be determined.

2.0 Methodology

2.1 Petrography and Textural Characterization

To determine the age of deformation events within the samples, the deformation textures must first be observed. This initial characterization of the textures helps to identify the sequence of deformation and a relative sense of the timing of metamorphic mineral growth. The monazite grains observed in the samples were then categorized based on the textural domain that they represent. To determine the orientation and extent of deformation within the samples, petrographic examination of these thin sections was carried out specifically targeting mineral relationships which indicate mineral assemblage and equilibrium (pressure and temperature) conditions. For example, staurolite porphyroblasts have textures and growth intervals indicative of polyphase deformation. Petrographic relationships act as a reconnaissance tool for detailed microprobe analyses. Collection of petrographic observations was performed at Dalhousie University.

2.2 EMP Analysis

The Electron Microprobe (EMP) is an important tool is geosciences as it allows observation and characterization of material on the micro- (μm) to nanometer (ηm) scale. This analysis can prove valuable in determining the compositional characteristics of minerals in-situ without the need for destructive and homogenizing chemical analysis. The EMP generates an accelerated beam of electrons with and energy range of 0.1-30keV which, through the use of electrical lenses, can be focused to spot sizes less than 1μm (Goldstein et al., 2003). This beam emerges from the gun and lenses and is focused into the sample chamber where it interacts with the sample to an approximate depth of penetration of 1μm (Goldstein et al., 2003). The

interaction of the electron beam and the sample produces x-ray signals characteristic of each element present. When detected, these x-ray signals provide useful information regarding the chemical composition of the sample material. This technique was used on monazite-bearing samples in the Robert MacKay Electron Microprobe Laboratory at Dalhousie University. The instrument is a JEOL JXA-8200 scanning electron microprobe.

One of the most critical aspects of microstructural monazite geochronology is the identification of all, or the majority of the monazite grains in a particular section to properly and accurately correlate the populations within a given structural setting (Williams and Jercinovic, 2002). This can prove difficult due to the relatively small size of monazite grains within metamorphic mineral assemblages. These monazite grains are commonly beyond the resolution of optical microscope observations alone. Identification of individual monazite grains for in-situ analysis is done using primarily two means: backscatter electron imaging and X-ray mapping. Chemical analysis is performed following the production of these identification tools.

2.21 BSE Imaging

Back scatter electrons (BSE) are those which were sourced by the beam and have been intercepted by a target surface but have not imparted energy to the sample. These electrons undergo a change in trajectory and escape the specimen in question. This process is quantified by the backscatter coefficient (η) defined as follows;

$$\eta = \frac{\eta BSE}{\eta B} = \frac{iBSE}{iB}$$

with ηB and ηBSE representing the number of incident beam electrons on the sample and the number of backscattered electrons respectively, while *i*B and *i*BSE refer to the electrical current

of the electron beam injected into the sample and current of the BSE passing through the sample (Goldstein et al., 2003). The important aspect of BSE imaging in material science is the dependence that is evident between η and the atomic number (*Z*) of the target sample (Lloyd, 1999). The relationship from an experimental point of view is that the intensity/brightness of the image increases corresponding with greater *Z* (Lloyd, 1999). When imaging a thin section there is clearly a highly variable compositional framework which results in a polyphase *Z* value for the section as a whole. As monazite and other REE-bearing minerals contain components with high *Z*, these minerals appear bright relative to the surrounding minerals. By decreasing the intensity of the BSE image, minerals with low *Z* appear dark and can be removed from the image leaving the relatively bright monazite highlighted and easily identifiable.

This technique allows for ease in identification of monazite grains within a sample but is limited due to the inability of BSE images to determine specific chemical compositions beyond atomic number contrast. For this, further analysis of the sample is needed.

2.22 X-Ray Mapping

Once the individual grains of monazite have been identified through the use of BSE imaging, the location and distribution of compositional domains within the monazite must be determined. To achieve this, x-ray maps can be produced to show the distinct chemical signature of the individual domains. X-ray maps are produced as a result of the interaction of the electron beam with the chemical components of the sample. The electron beam excites a portion of the electrons within the sample which in turn release this energy in the form of x-rays. In the study of monazite, the elements that are targeted are P, Y, Ce, Th and Ca. These elements are important due to the reactions that form monazite. These elements are concentrated in monazite

overgrowths during the breakdown of minerals in tectono-metamorphic settings. Then x-rays are measured and characterized on the basis of wavelength. The wavelength of these x-rays when analyzed can be used to determine the element from which they were produced. By combining the determined elemental compositions from the complete grain, a compositional map of the grain can be produced which has the individual domains identified. These maps can be interpreted in terms of the domains present which formed during separate metamorphic events. Once domains have been identified, the chemical ratios of U, Th and Pb are used in geochronologic equations to determine the age of these deformation events.

2.23 Major and Trace Element Analysis

X-ray maps are qualitative and show the distributions of elements. These data can be used to infer textures and reactions within an individual sample. Expanding on these maps, single spot analysis will provide accurate, precise and complete signatures of the chemical composition within each domain. These chemical compositions are used to determine the reactive character of the monazite grain which constrains the specific P-T conditions experienced by the host rock, which in turn defines the parameters of deformation during the individual monazite growth phases. Specifically, this study uses the relationship of REE within monazite and xenotime. Previous research has proven that partitioning of REEs between monazite and xenotime is temperature-dependent, allowing for geothermometric calculations (Andrehs and Heinrich, 1998). Through chemical analysis and distribution of REEs within individual compositional domain, the formation conditions can be accurately determined. Beyond this method, the Y distribution between monazite and garnet also characterizes the geothermometric conditions of the sample (Pyle et al., 2001). This method is performed similarly to the previous geothermometric procedure although only the distribution of Y is targeted. This distribution

determines whether the monazite grew at the expense of garnet which constrains the P-T setting during formation due to equilibrium conditions. These data also allow for more accurate determination of trace-elements, in particular Pb and U, which is used in the determination of age ranges for the individual monazite domains that proxy separate deformation events.

Determination of trace-element components requires an increase in count time and beam current as the quantities of these elements are so low they are likely to be obscured during the analysis by the peak counts of major-element components (Williams et al., 2006). These amplified factors increase the quantity of x-ray emissions from the sample and the amount of time available for measurement collection. This increase is coupled with a normalizing factor of a major-element (for Pb in monazite, the normalizing major-element constituent is Ce) to improve resolution. These parameters combine to improve the accuracy of trace-element measurements.

3.0 Petrography and Chemical Analysis

3.1 General Statement

The samples used in this study were collected as part of a project investigating low pressure metamorphism in the Meguma Terrane by Dr. R.A. Raeside and Dr. Rebecca Jamieson of Acadia and Dalhousie Universities, respectively. Thin-section microscopy was completed on four samples, two representative of the Government Point Formation of the Goldenville Group and two representing the Cunard Formation of the Halifax Group with the purpose of: (1) documenting the mineral assemblage present in the study area, (2) evaluating and describing the metamorphic textures, and (3) constraining the textural domains representative of separate but linked deformation events which are preserved within the samples. The thin-section microscopy was supported through the use of the scanning electron microprobe to analyze the chemical signature of monazite grains in the samples. This chapter presents detailed petrographic description of samples collected in the study area as well as chemical characterization of analyzed monazite grains.

3.2 Petrographic Description

For clarity, the following table outlines the sequence of mineral growth phases which can be identified in the analyzed samples. The events are listed chronologically as they are preserved. It should be noted that the effects of contact metamorphism vary with distance from the intruding body which explains the growth of staurolite and andalusite while also preserving the original schistosity in samples SWM-13 and -14. The stability ranges of garnet and biotite allow for multiple phases of growth which becomes evident when porphyroblast-matrix foliation relationships are considered (Fig.8).

Metamorphic Phase (age)	Mineral Assemblage	Associated Fabric/Texture
Protolith (Pre-Metamorphism)	Tubiditic Sandstone	N/A
Acadian Orogeny Deformation (400-380Ma)	Grt+Bt+Qtz+Pl+Ms	Mica-Defined Schistosity
Contact Metamorphism (≈370Ma)	Qtz+Pl+Ms+Rt+St+And±Cd	Equigranular Matrix Grains
Retrogression (<320Ma)	Qtz+Pl+Ms+Cl+And+Grt+Rt	Pseudomorphic Replacement

Table 2: Interpreted metamorphic history of analyzed samples identifying relative chronology of mineral growth.

3.21 Sample SWM-8

This sample was collected from Sandy Point, located approximately 12km south of Shelburne, NS (location SWM-8 in Fig.2) which has been classified in the field as a staurolite-andalusite schist. The original mineral assemblage of this sample is characterized by a garnet+biotite+quartz+plagioclase+muscovite+rutile. This primary mineralogy is overprinted by a higher order metamorphic assemblage including staurolite and andalusite in the same way as sample SWM-6.

Due to the stability range of both biotite and garnet, the growth of these minerals likely spans from the early stages of metamorphism to much later events which explains the apparent multi-generational growth of these minerals. This variation in growth timing is preserved in the internal texture of garnet as well as the inclusions of biotite and garnet within staurolite and andalusite (Fig.4). As the microphotograph indicates, there was a leading porphyroblast growing event which produced garnet. This garnet growth would have coincided with the original growth of biotite although this is not observed in Figure 6. This phase of porphyroblast growth was followed by and overprinted by the growth of staurolite and andalusite as a result of contact metamorphism produced by the granitic intrusions. The staurolite porphyroblasts of this sample display a pronounced oscillatory zonation which is interpreted to represent a stage of biotite

breakdown contributing to the growth of staurolite (Fig.5). There is a distinct compositional banding preserved within this sample defined by sections of predominantly matrix grains and biotite porphyroblasts distinct from sections dominated by relatively small garnet porphyroblasts. The matrix grains of this sample are quartz, plagioclase, muscovite and rutile and display elongate and aligned forms which, when taken in association with the general alignment of biotite porphyroblasts, defines a weak schistosity. The development of this fabric appears to have taken place prior to the growth of staurolite and andalusite indicating separate phases of equilibrium conditions during prograde metamorphism. Following the periods of foliation development and porphryoblast growth a stage of the retrogression took place identified by replacement of staurolite by chlorite and muscovite which is also present in sample SWM-6.

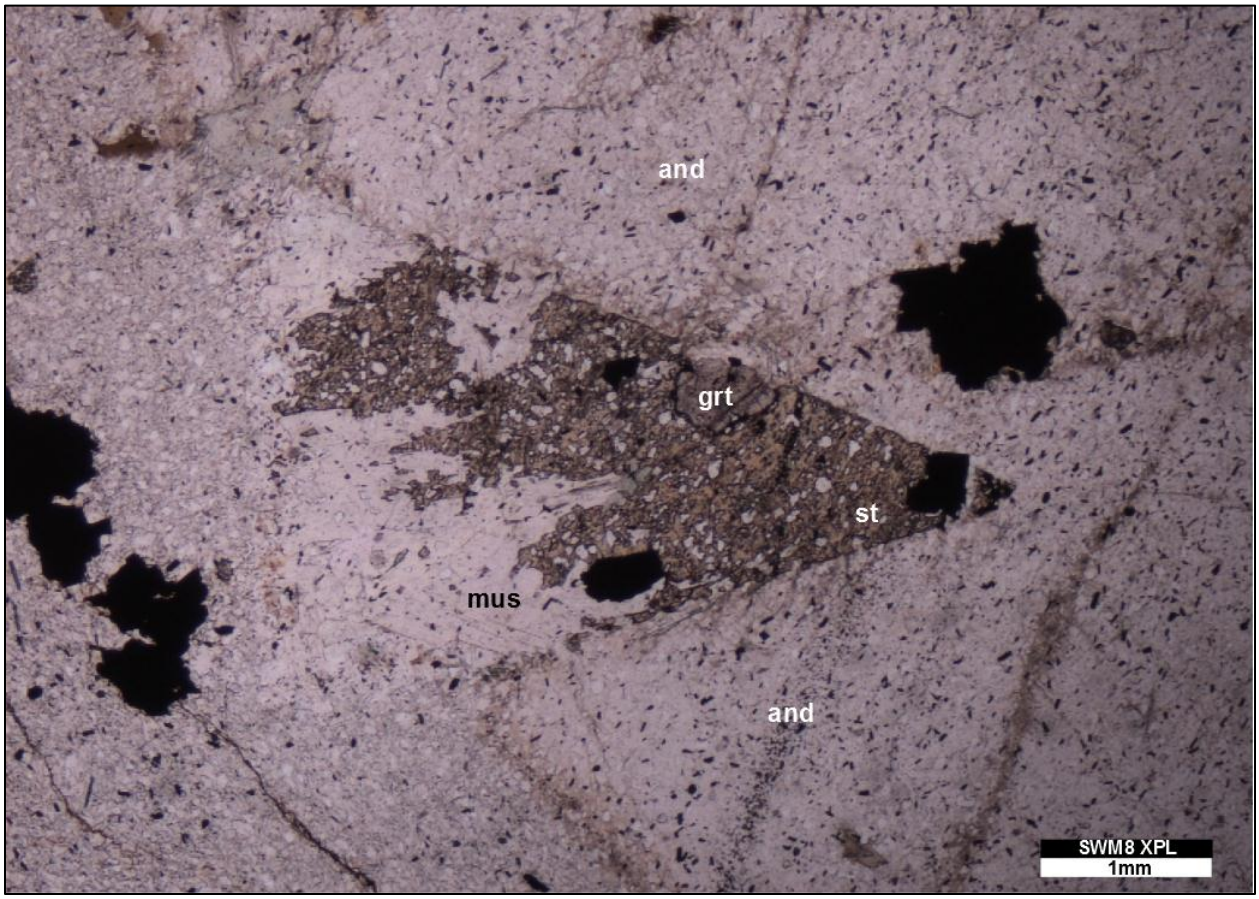

Fig.4: Porphyroblast-inclusion relationship between early-stage garnet and later-stage overgrowth by staurolite and andalusite.

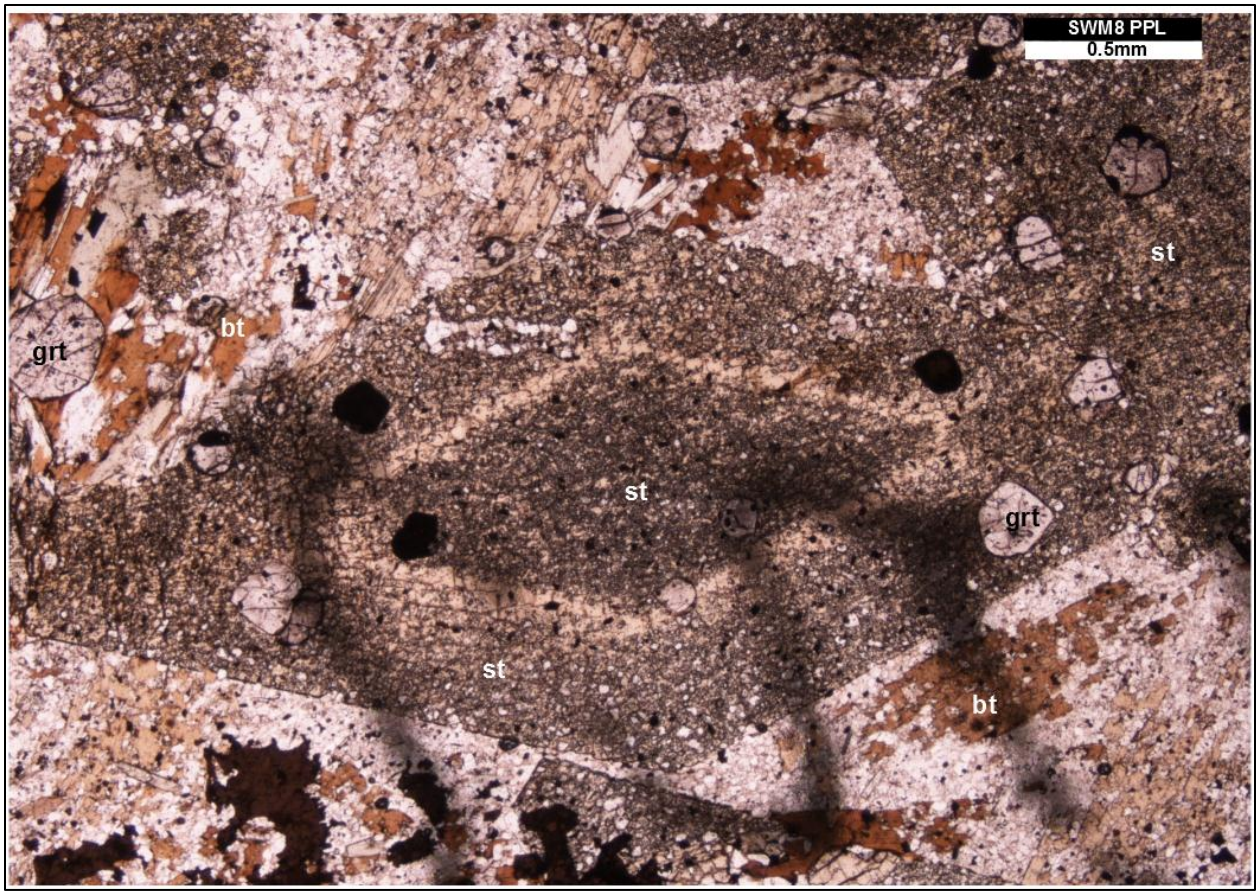

Fig.5: Oscillatory zonation of poikiloblastic staurolite.

3.22 Sample SWM-6

This sample is representative of the Government Point Formation. It was collected from Jordan Falls in an outcrop described as a staurolite-andalusite metacrystic pelite. This sample is characterized by a garnet+biotite+quartz+plagioclase+rutile mineral assemblage which has an overprinted by poikiloblastic staurolite and andalusite along with accessory cordierite. This mineral assemblage places the sample within the amphibolite metamorphic facies and gives an approximation of the temperature and pressure conditions during crystal growth. The conditions of this sample are interpreted to be applicable for all samples analyzed. There is a weakly defined schistosity identified by the relative alignment of equigranular matrix plagioclase and rutile grains. The porphyroblasts of biotite display no relative alignment corresponding to the

orientation of the matrix. The staurolite poikiloblasts observed in this sample occur in two distinct forms, those in the matrix which contain inclusions of quartz and graphite and those which were produced by the replacement of biotite which are inclusion-poor (Fig.4). This texture gives insight into the metamorphic history of the sample suggesting that the biotite porphyroblasts were present prior to the growth of staurolite. Comparatively, the andalusite in this sample appears to have replaced the matrix plagioclase and muscovite while leaving the rutile and garnet unaffected again suggesting that both the andalusite and staurolite grew due to a later stage metamorphism following the development of the foliation. Of all samples analyzed, the retrograde metamorphism is most pronounced in SWM-6 with the replacement of euhedral staurolite by muscovite (Fig.5) and the growth of chlorite at the expense of biotite

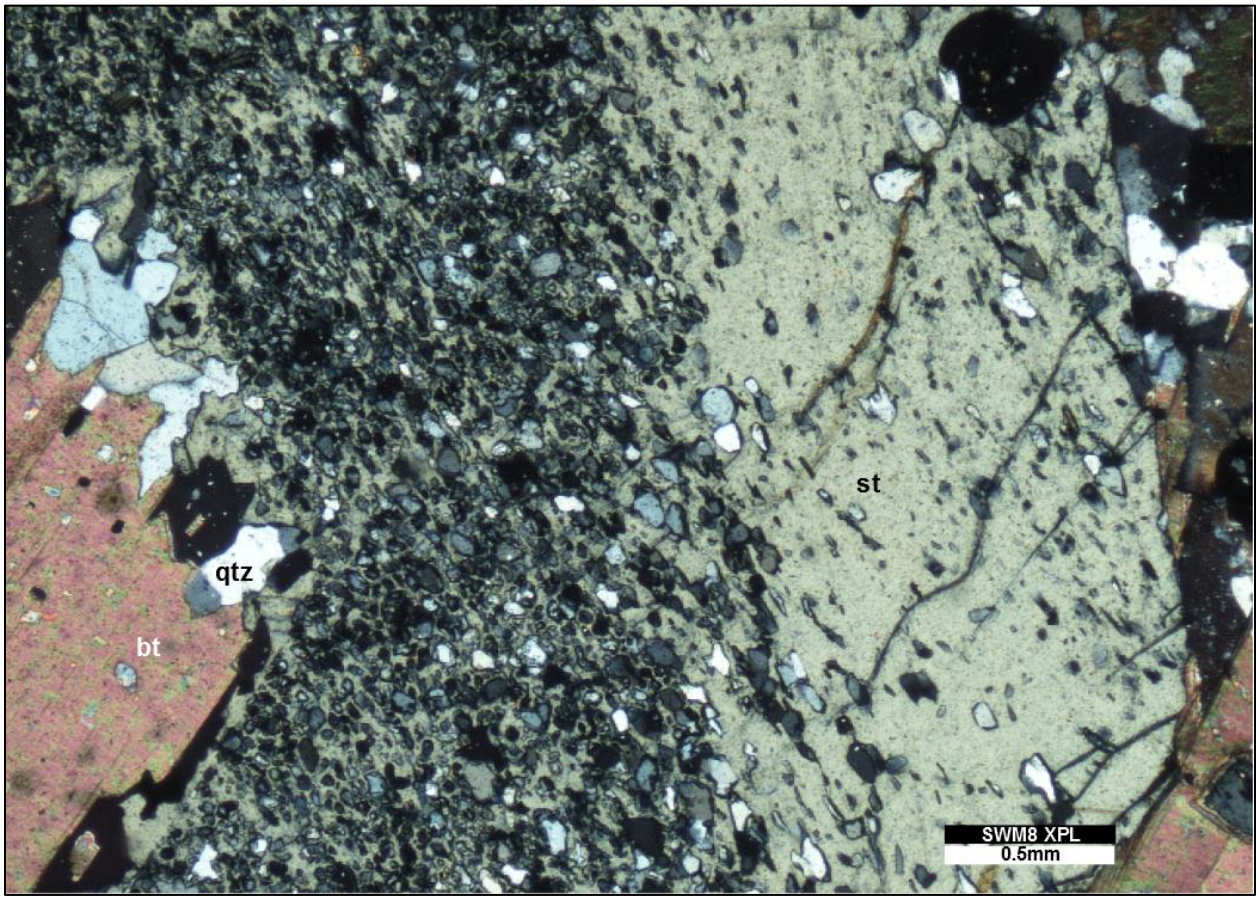

Fig.6: Staurolite porphyroblast displaying both poikilolitic and inclusion-poor form.

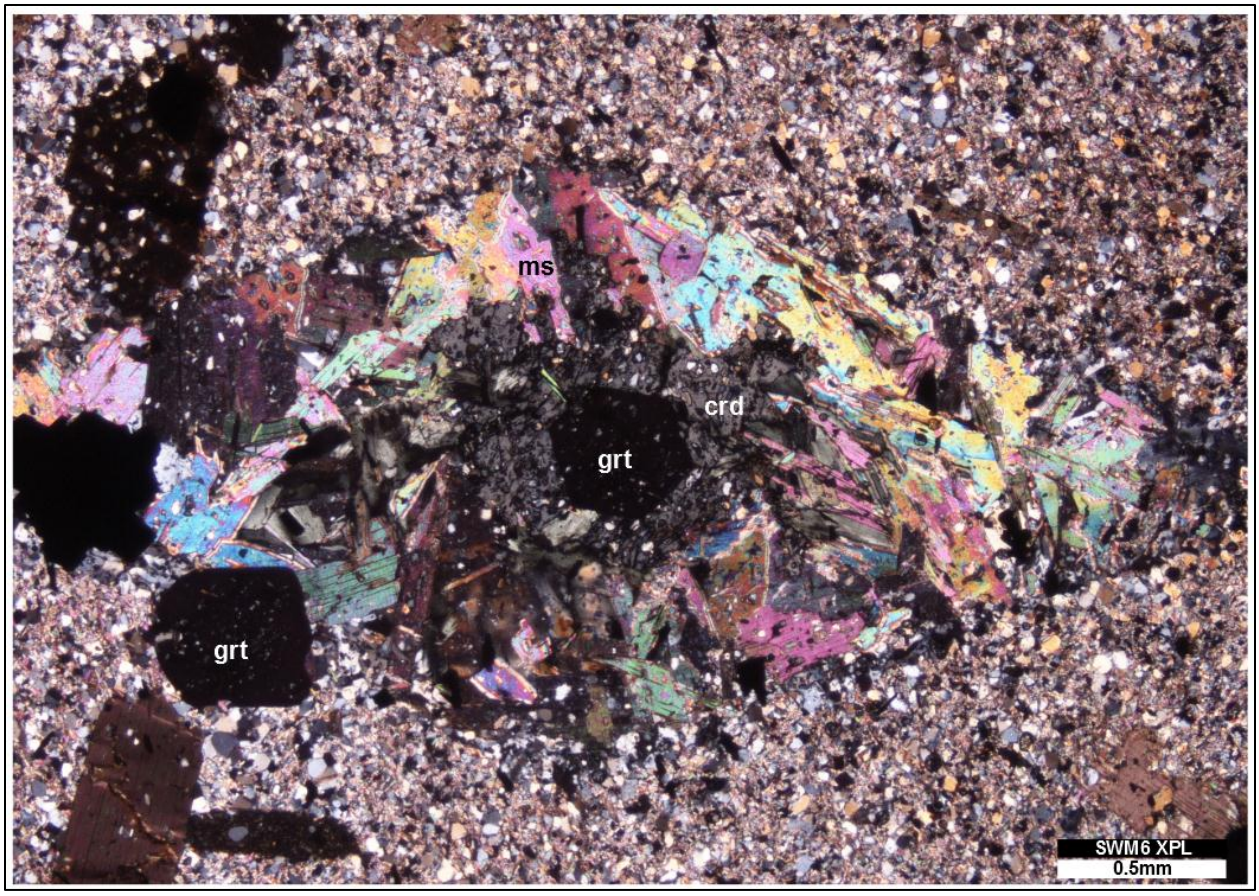

Fig.7: Pseudomorphic replacement of a euhdral staurolite porphyroblast by muscovite.

3.23 Sample SWM-13

This sample is geographically distinct from the previous examples as it was collected in the region of Lower West Pubnico from an outcrop classified as a chiastolite (andalutsite)-bearing slate. Unlike the previous samples, SWM-13 represents the Cunard Formation of the Halifax Group, straigraphically overlying the Goldenville in southern Nova Scotia. The mineral assemblage of this sample is consistent with that of the previous samples, being represented by garnet+biotite+quartz+plagioclase+muscovite+rutile and subsequently overprinted by staurolite and andalusite. The key feature of the mineralogy in this sample is the abundance and large relative size of cordierite. A defining characteristic of this sample is the compositional banding identified by the presence and absence of porphyroblasts resulting in regions consisting solely of

matrix grains. This is likely a relict feature representing the compositional differences which were present in the original sedimentary unit. There is a well-defined foliation fabric preserved in this sample which is identified by biotite as well as the alignment of matrix grains observed in previous samples (Fig.8). Retrograde reactions are present in this sample as well as in SWM-14 although it is less significant and identified by the growth of chlorite at the expense of staurolite and biotite porphyroblasts (Fig.9).

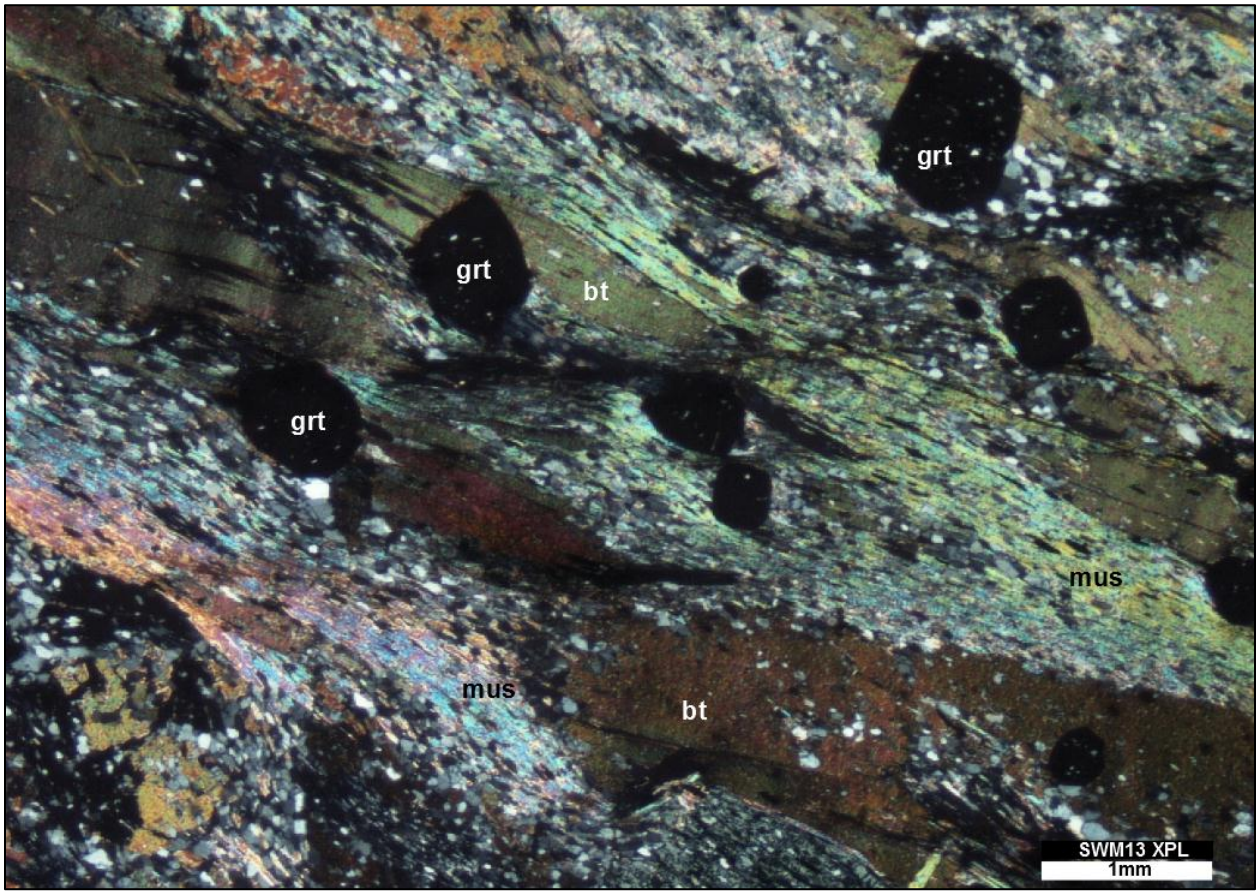

Fig.8: Mica-defined foliation fabric. Notice the wrapping texture around garnet porphyroblasts while in other cases being overprinted indicating multiple growth phases of garnet.

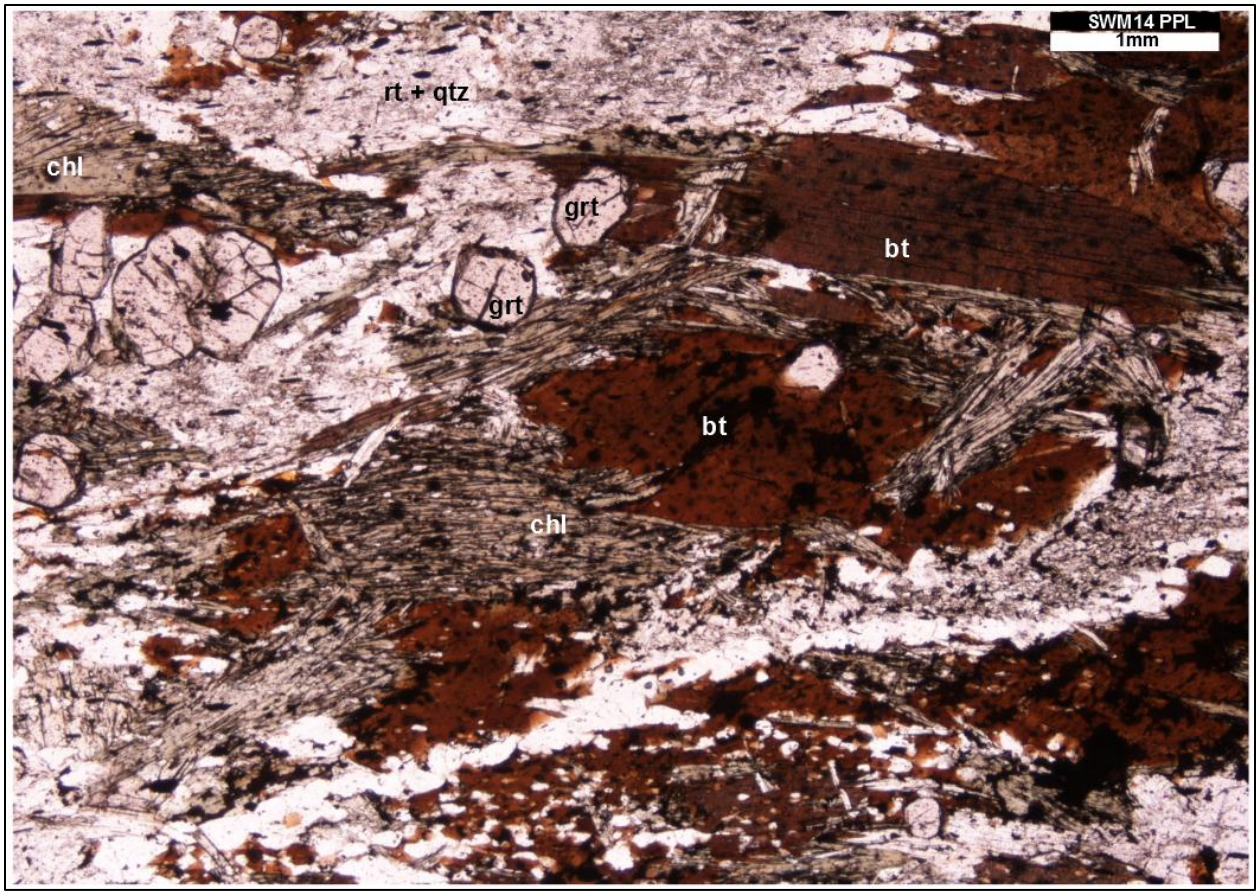

Fig.9: Retrograde reaction texture yielding chlorite at the expense of biotite porphyroblasts.

3.24 Sample SWM-14

This sample again represents the Cunard Formation of the Halifax Group and was collected from the Pubnico Point peninsula on the southern coast of Nova Scotia. This outcrop is defined as a coarse-grain andalusite schist and has a similar mineral assemblage as the previous samples although andalusite is dominant while cordierite is relegated to a minor component. The most striking feature of this sample is the pervasive muscovite- and biotite-defined schistosity which is far more pronounced than the relative alignment of matrix grains observed in previous samples (Fig.10). This deformation fabric however is subject to compositional banding which separates it from sections characterized by an equigranular, relatively fabric-free matrix. Garnet porphyroblasts in this sample generally display an equant texture while containing numerous

quartz inclusions which defines an internal fabric. This internal fabric is relatively aligned with the foliation observed in the matrix but in particular specimens is slightly oblique to the foliation. This texture is interpreted to represent rotation of the porphyroblast immediately following crystallization. The garnet growth is part of the same metamorphic event but represents the earliest stages of deformation due to the absence of an identifiable rotation fabric surrounding the porphyroblast. Contradicting this is the presence of garnet porphyroblasts which are highly resorbed and do not contain inclusions. These garnets clearly represent an earlier stage growth that has undergone subsequent reactions, likely during the growth of staurolite.

Fig.10: Distinct quartz- and mica-defined foliation fabric evident in sample SWM-14.

3.25 Summary of Metamorphic Conditions

Based on the mineral assemblage observed within the samples, the metamorphic conditions can be inferred. The peak metamorphic grade of the analyzed samples is identified by the presence of staurolite and andalusite. As mentioned earlier, these minerals grew due to contact metamorphism and place the samples within the amphibolite metamorphic facies under conditions of approx. 550-600°C and 2.5 kb (Fig.11) which would facilitate the recrystallization and growth of monazite. Conversely, the earlier-phase, foliation-forming deformation appears to have only reached the garnet zone indicating the conditions were below that of the contact metamorphism. These conditions are at the lower limit of monazite growth and stability contributing to the preservation of detrital grains within the analyzed samples.

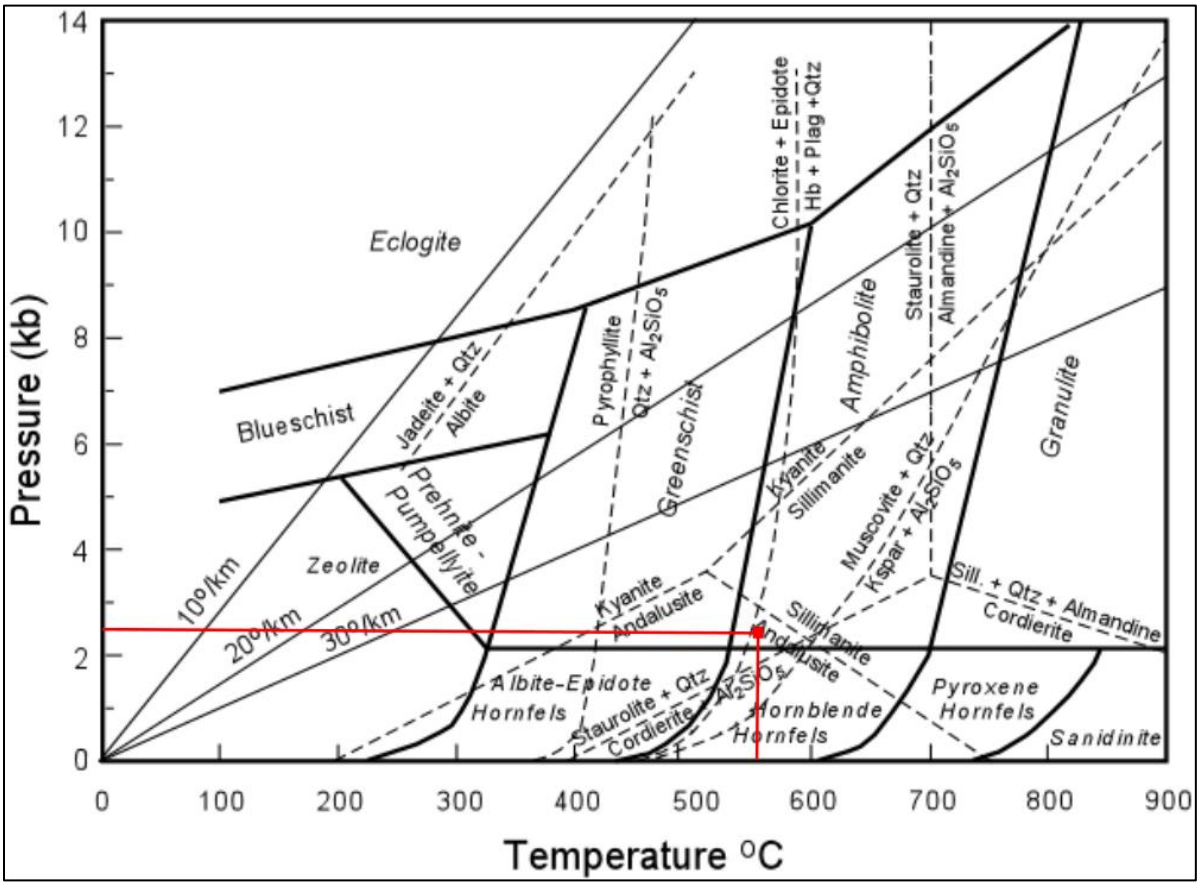

Fig.11: Peak metamorphic conditions interpreted from the preserved mineral assemblage. These conditions are supported HREE-distribution in monazite and xenotime grains (modified after Winter, 2010).

3.3 Monazite Texture & Chemistry

3.31 Textual Interpretation

Monazite grains within the analyzed samples can be categorized into one of two domains defined by textural relationships. The first of these domains encompasses monazites hosted within porphyroblasts of biotite and staurolite. This domain of monazite is particularly evident within samples SWM-8 and SWM-13 in which biotite porphyroblasts are well developed and prevalent. The monazites of this domain display a characteristic resorbed texture indicative of breakdown reactions associated with varying stages of metamorphic deformation. The products of this breakdown appear to be apatite and plagioclase which are characteristic of retrogression of monazite under low T and P conditions (Fig.12). This texture represents growth of monazite during an early metamorphic event followed by a breakdown resulting from a later stage, lower-magnitude metamorphism. As mentioned earlier, the growth of metamorphic monazite occurs due to the breakdown of phosphate minerals or garnet which act as sources of REE's. Due to the equant crystal shape of garnet porphyroblasts in the samples, it can be proposed that the monazite and garnet developed in equilibrium which suggests early-stage phosphates as the metamorphic source of monazite growth.

The second domain of monazites within the analyzed samples describes those hosted in the matrix associated with elongate quartz and rutile. The monazites representative of this domain are abundant in sample SWM-6. This domain is characterized by relatively small (approx. 5μm diameter) and euhedral monazites aligned with the schistosity of the sample. These monazites are typically associated with rutile and quartz which characterize the matrix and this should be expected as per the reaction of titanite and a phosphate source listed previously. The

interpretation of this textural dichotomy is a relicted monazite grains which have been subsequently overprinted by the staurolite and foliation-forming metamorphic deformation which contributed to the growth of the matrix-hosted monazites. The biotite porphyroblasts served to protect the primary monazite from the effects of the deformation.

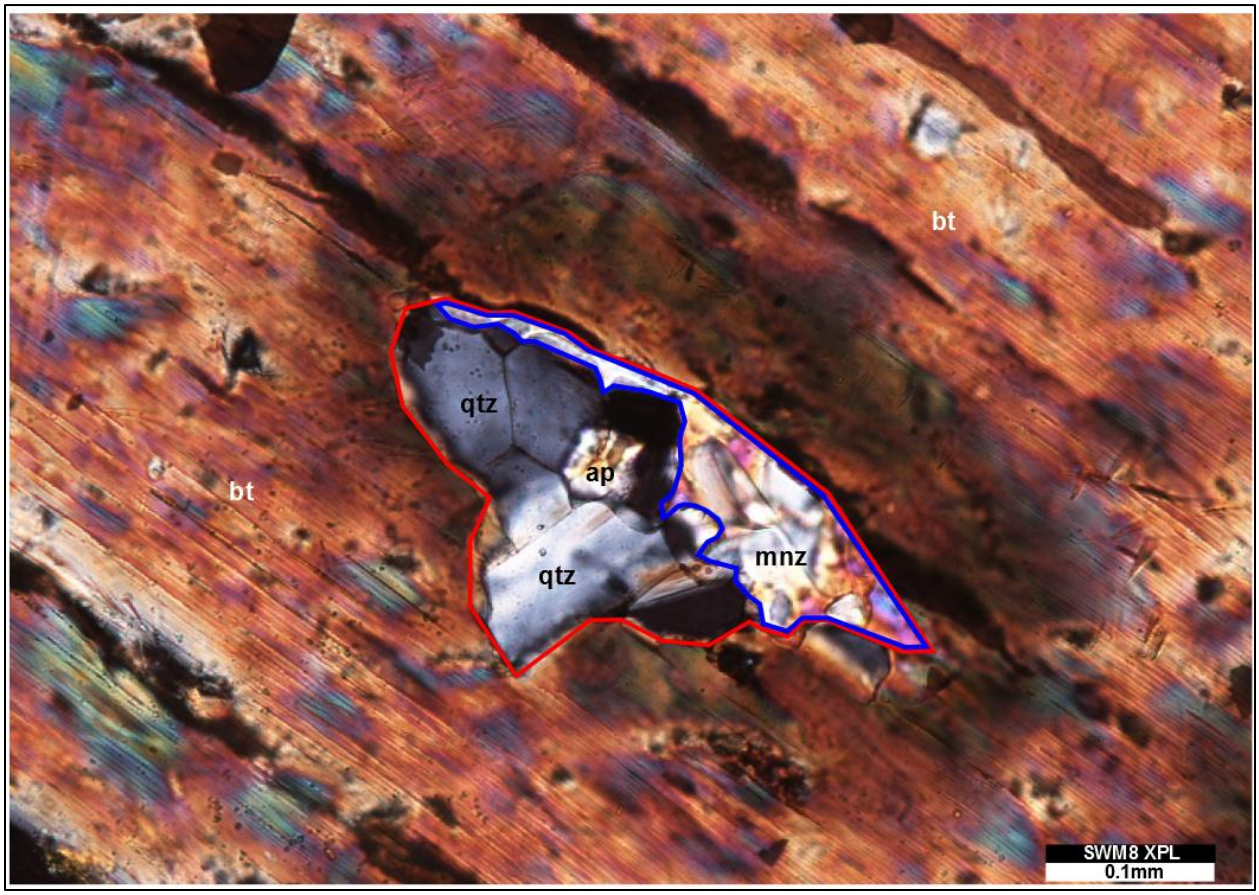

Fig.12: Biotite porphyroblast-hosted monazite displaying metamorphic overprinting texture identified by the breakdown yielding qtz and ap. Pre-deformation shape highlighted in red, resorbed and present shape in blue.

3.32 Chemical Characterization

Chemical analysis was performed on the monazite grains identified within the samples. These chemical data provide insight into the growth of the monazites as well as defining separate domains which classify the individual monazites. Trace chemical data is presented in Appendix

I. The analysis of monazite grains shows a characteristic enrichment in LREE, particularly Ce and La, Based on the end-member classification of monazites proposed by Lithout (2007), the monazites of these samples are overwhelmingly of the (REE)-Monazite series (Fig.13) which supports the theory of primary phosphate breakdown during metamorphism (abundance of PO_4 as opposed to Th or Si). This plot was produced using Triplot software. The chemical analysis yields information which supports the textural domain classification. When analyzed using the x-ray mapping feature of the electron microprobe, it becomes obvious that the resorbed, porphyroblast-hosted monazites display a characteristic zonation identified by relative proportions of Th and Y specifically the concentration of Th in the core of the grain while Y levels are elevated in the rim (Fig.14). This chemical signature is not however observed in the matrix grains. As noted in Figure 15, the matrix grains are homogeneously enriched in Y without the Th-rich core observed in porphryoblast-hosted samples. One would expect chemical homogeneity during individual growth events as the chemical components which form the mineral would be in equilibrium during this time. Because of this, the interpretation is that the chemically distinct zones within monazite grains represent periods of recrystallization under differing equilibrium conditions.

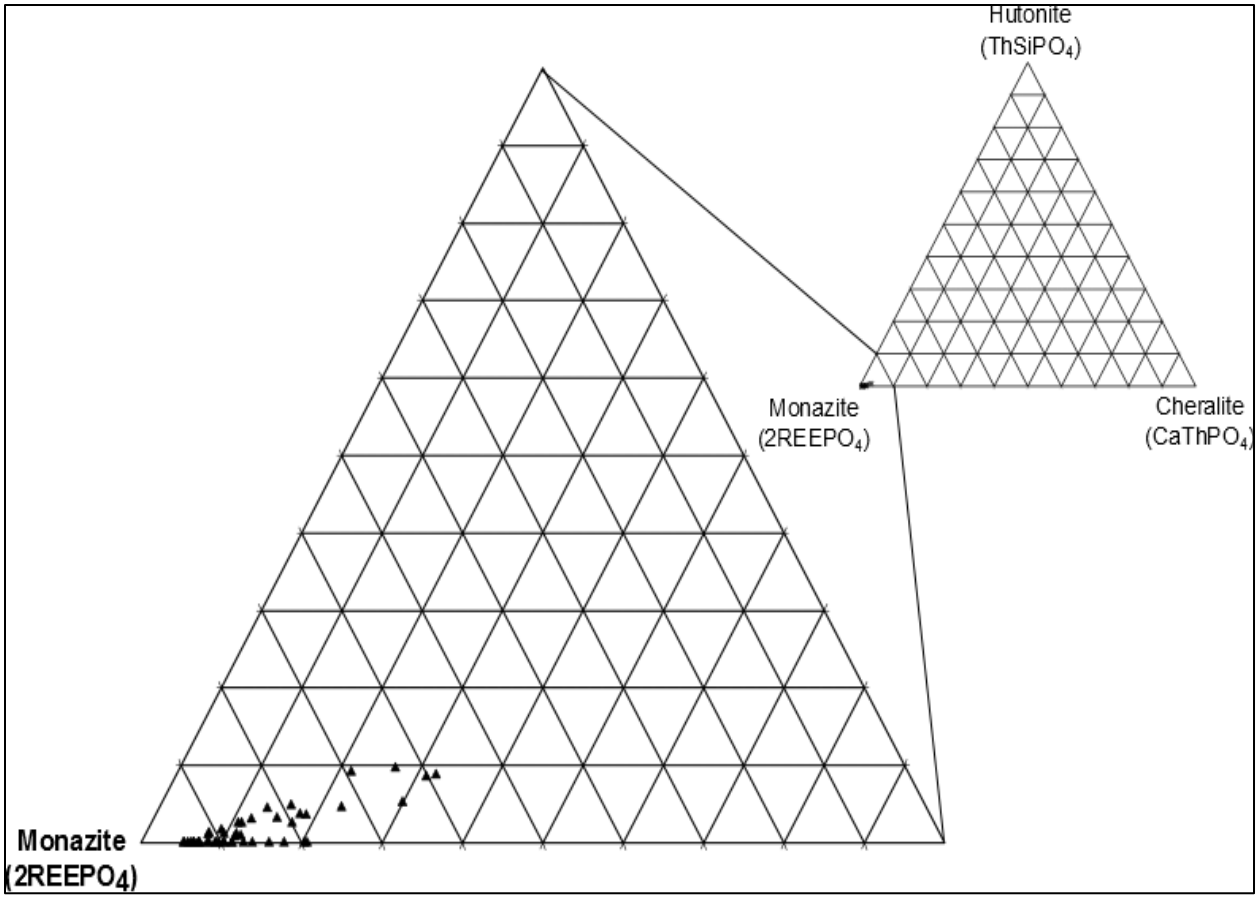

Fig.13: Ternary plot identifying the end-member series of chemically analyzed monazite grains. The samples display a significantly skewed distribution towards the (LREE)-Monazite series.

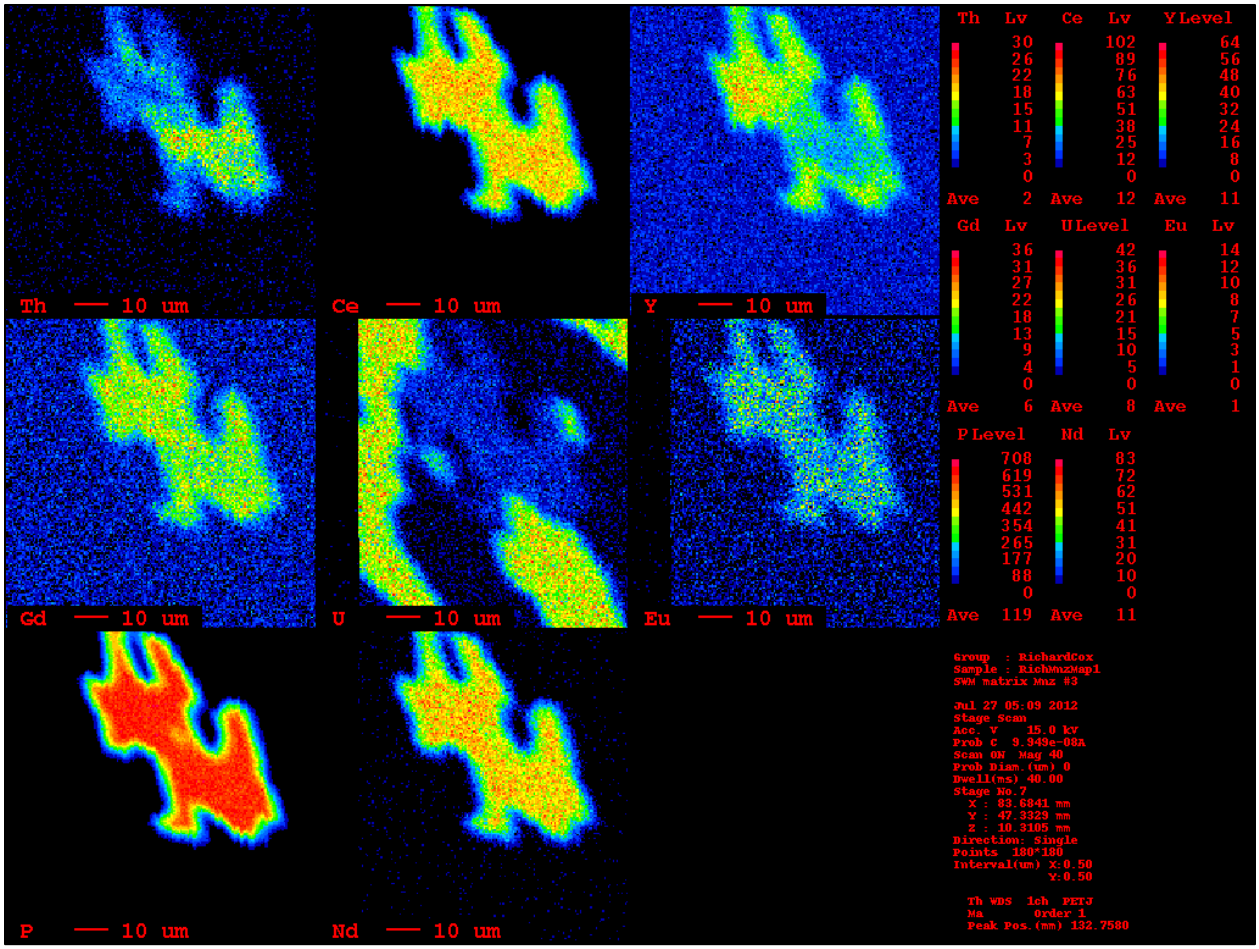

Fig.14: X-ray map identifying Th-rich core and Y-rich rim of resorbed matrix-hosted monazite grain of sample SWM-8.

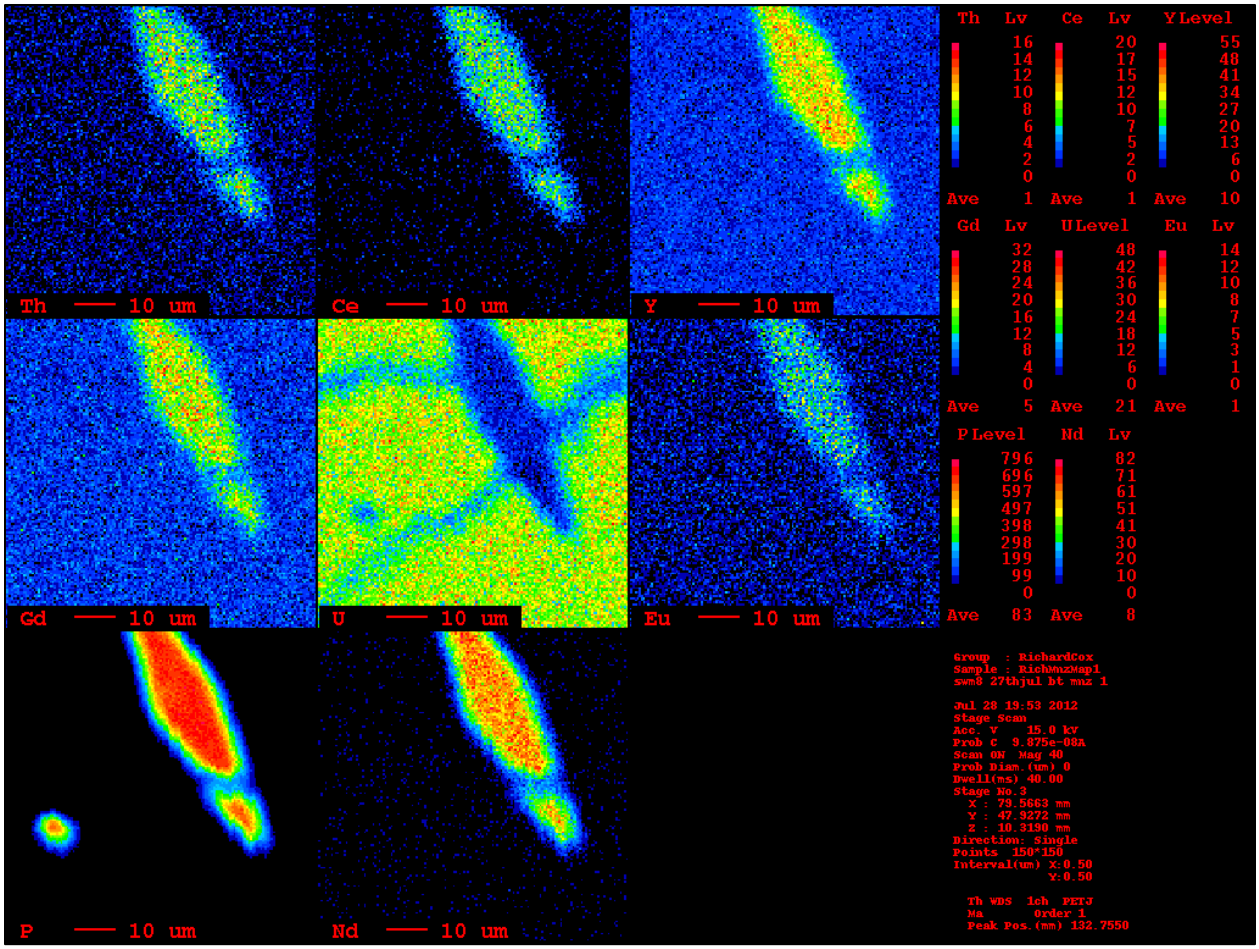

Fig.15: X-ray map of matrix-hosted, foliation-alligned monazite grain in sample SWM-8 displaying homogenous Y-enrichment while lacking a Th-rich core.

4.0 Results of U-Th-Pb Dating

4.1 General Statement

Upon identification and chemical characterization of the monazite grains within the samples, higher energy current was employed to determine the specific concentrations of U, Th, Y and Pb. These elements are used to determine the age when the monazite was thermally closed thermodynamically limiting diffusion of elements (specifically Pb) within the crystal structure. While U, Th and Y occur with relatively high abundance (in the case of Th as much as 10 wt.%), total Pb in the samples is minor requiring specialized analytical techniques to determine with accuracy. The means of collecting this data requires doubly coating polished sections with carbon to protect from the high current and longer exposure time. During normal analysis, the electron microprobe emits a current of 20 nanoamps and spot exposure duration is typically 3min. For the collection of Pb peaks however, the current amperage is increased to 200 nanoamps and time of exposure is 18min. per spot analysis. With the concentrations measured (in ppm), these values are processed using the age calculation listed in the introduction. To perform this calculation, spreadsheet analysis was performed using the method originally formulated by Montel (1990) followed by probability distribution developed using isoplot. To ensure accuracy in measurement, standard monazites of known composition and age were analyzed to determine interference parameters. The standards utilized in this study are of the Geologic Survey of Canada (GSC) sample set and are representative of Elk Mountain, New Mexico and Jefferson County, Colorado. The documented age of these samples is 550 Ma (Elk Mountain) and 350 (Jefferson County) and analysis of the standards yielded age range of 514-535 Ma and 320-345 Ma respectively (Kelts et al., 2008). The results of this analysis indicate

that the measurements were producing accurate values (Appendix I). Intermittent retesting of these standards was performed to identify potential drift in the set elemental peaks.

4.2 Chemical Ages

Chemical analysis was performed on 62 monazite grains identified in samples SWM-6,-8 and -13 (no monazites were observed in SWM-14). Complete analysis is presented in Appendix I. The measured U, Th, Y and Pb values along with the associated ages and errors calculated are noted as follows.

SWM6										
	Th (ppm)	err	U (ppm)	err	Pb (ppm)	err	age (Ma)	err	Pb Det. Lim.	Age Det. Lim.
SWM6 Mtx Mnz1 pt1	30270	242	2870	13	650	9	**368**	**8**	2	90
SWM6 Mtx Mnz2 pt1	35760	259	3120	16	760	11	**370**	**8**	1	119
SWM6 Mtx Mnz3 pt1	56170	429	7620	34	1340	20	**370**	**8**	7	90
SWM6 Mtx Mnz5 pt1	61080	459	550	3	1030	15	**366**	**8**	4	106
SWM6 Mtx Mnz6 pt1	30260	243	3070	16	660	10	**367**	**8**	3	60
SWM6 Mtx Mnz7 pt1	39280	304	5810	30	970	14	**373**	**8**	4	88
SWM6 Mtx Mnz8 pt1	12420	91	12550	46	810	12	**342**	**6**	3	87
SWM6 Mtx Mnz9 pt1	41450	320	3510	375	890	13	**376**	**16**	3	98
SWM6 Mtx Mnz10 pt1	12460	97	7500	33	610	9	**371**	**7**	2	104
SWM6 Mtx Mnz11 pt1	27640	224	4490	549	710	10	**376**	**22**	4	57

Table 3a: Results of chemical analysis and age calculation for monazite grains in sample SWM-6. Mtx-matrix, Mnz-monazite.

SWM8										
	Th (ppm)	err	U (ppm)	err	Pb (ppm)	err	age (Ma)	err	Pb Det. Lim.	Age Det. Lim.
SWM 8 Bt Mnz3 pt1	31230	258	3820	17	920	13	**470**	**10**	3	99
SWM 8 Bt Mnz3 pt2	50490	396	3820	16	1350	19	**478**	**10**	5	90
SWM 8 Bt Mnz3 pt3	55150	433	4120	18	1580	23	**513**	**11**	6	119
SWM 8 Bt Mnz3 pt4	43380	334	3300	14	1070	15	**440**	**9**	4	90
SWM 8 Bt Mnz3 pt5	13870	108	3340	15	740	11	**658**	**13**	3	106
SWM 8 Mtx Mnz2 pt1	15680	127	1950	9	640	9	**642**	**13**	2	60

SWM 8 Mtx Mnz2 pt2	27330	213	3000	13	950	14	**568**	**12**	4	88
SWM 8 Mtx Mnz2 pt3	44940	342	7150	31	1470	21	**480**	**10**	6	87
SWM 8 Mtx Mnz2 pt4	46260	368	6190	27	1280	18	**430**	**9**	5	98
SWM 8 Mtx Mnz2 pt5	18740	151	2530	11	2320	33	**1000**	**32**	9	104
SWM 8 Mtx Mnz2 pt6	45280	349	3780	16	1310	19	**506**	**11**	5	57
SWM 8 Bt Mnz1 pt1	17830	139	2110	9	760	11	**679**	**14**	3	95
SWM 8 Bt Mnz1 pt2	20870	167	2380	11	590	8	**459**	**10**	2	59
SWM 8 Bt Mnz1 pt3	30080	232	2860	13	780	11	**441**	**9**	3	59
SWM 8 Bt Mnz1 pt4	36930	286	3200	14	1170	17	**549**	**11**	4	59
SWM 8 Bt Mnz1 pt5	14640	114	2050	9	750	11	**772**	**16**	3	59
SWM 8 Mtx Mnz3 pt1	41060	308	3000	13	1180	17	**516**	**11**	4	59
SWM 8 Mtx Mnz3 pt2	67930	516	3270	14	1880	27	**532**	**11**	7	59
SWM 8 Mtx Mnz3 pt3	51660	397	3430	15	1390	20	**492**	**10**	5	59
SWM 8 Mtx Mnz3 pt4	86320	649	4910	21	1990	29	**434**	**9**	7	59
SWM 8 Mtx Mnz3 pt5	42100	318	3470	15	1230	18	**512**	**11**	4	59
SWM 8 Mtx Mnz3 pt6	32660	253	4600	20	1060	15	**495**	**10**	4	59
SWM 8 Bt Mnz2 pt1	44350	334	4380	19	1240	18	**471**	**10**	5	59
SWM 8 Bt Mnz2 pt2	33160	255	2790	12	690	10	**365**	**8**	3	59
SWM 8 Bt Mnz2 pt3	12860	106	1770	8	420	6	**502**	**10**	2	59
SWM 8 Bt Mnz2 pt4	19280	152	2120	10	650	9	**550**	**11**	2	59
SWM 8 Bt Mnz2 pt5	21490	170	2920	13	750	11	**550**	**11**	2	59
SWM 8 Mtx Mnz5	41490	316	3620	16	1450	21	**537**	**11**	3	59
SWM 8 Mtx Mnz6	30910	242	2460	11	1330	19	**603**	**12**	5	59
SWM 8 Mtx Mnz7	47720	380	3280	14	1520	22	**752**	**16**	5	59
SWM 8 Mtx Mnz8	27700	216	3410	15	1190	17	**577**	**12**	5	59
SWM 8 Mtx Mnz9	28980	219	3320	15	1060	15	**676**	**14**	4	59
SWM 8 Bt Mnz4 pt3	24820	145	2940	88	1100	95	**590**	**12**	4	59
SWM 8 Bt Mnz4 pt1	36790	215	3610	108	1220	106	**704**	**67**	169	59
SWM 8 Bt Mnz4 pt2	14410	84	1750	52	570	49	**558**	**53**	187	59
SWM 8 Mtx Mnz10	78120	622	3660	16	1690	24	**419**	**9**	6	90
SWM 8 Mtx Mnz11	58320	463	5340	24	1390	20	**410**	**9**	6	119
SWM 8 Mtx Mnz12	62540	491	3820	17	1200	17	**358**	**8**	5	90
SWM 8 Mtx Mnz13	28160	216	2980	12	830	12	**488**	**10**	3	106
SWM 8 Mtx Mnz14	30950	242	2810	12	820	12	**456**	**10**	4	60
SWM 8 Mtx Mnz15	26280	195	3290	14	760	11	**458**	**9**	3	88
SWM 8 Mtx Mnz16	27250	242	2970	12	700	10	**423**	**9**	2	87
SWM 8 Mtx Mnz17	46120	376	3210	14	1030	15	**407**	**9**	4	98

Table 3b: Results of chemical analysis and age calculation for monazite grains in sample SWM-8. Bt-biotite

SWM13										
	Th (ppm)	err	U (ppm)	err	Pb (ppm)	err	age (Ma)	err	Pb Det. Lim.	Age Det. Lim.
SWM13 MtxMnz1 pt1	41490	388	3620	18	1450	21	**603**	**13**	7	95
SWM13 MtxMnz1 pt2	30910	304	2460	12	1330	19	**752**	**17**	6	99
SWM13 MtxMnz1 pt3	47720	404	3280	15	1520	22	**577**	**13**	7	90
SWM13 MtxMnz4 pt1	27700	220	3410	16	1190	17	**676**	**14**	5	119
SWM13 MtxMnz4 pt2	28980	239	3320	16	1060	15	**590**	**12**	5	90
SWM13 MtxMnz4 pt3	32320	260	3570	17	1110	16	**560**	**12**	5	106
SWM13 MtxMnz5 pt1	33160	272	4430	21	1280	19	**595**	**12**	6	60
SWM13 MtxMnz5 pt2	24160	192	3480	17	1060	15	**659**	**14**	5	88
SWM13 MtxMnz5 pt3	23800	198	3480	17	1210	18	**756**	**16**	6	87

Table 3c: Results of chemical analysis and age calculation for monazite grains in sample SWM-13.

.

Below is the probability distribution for the calculated ages.

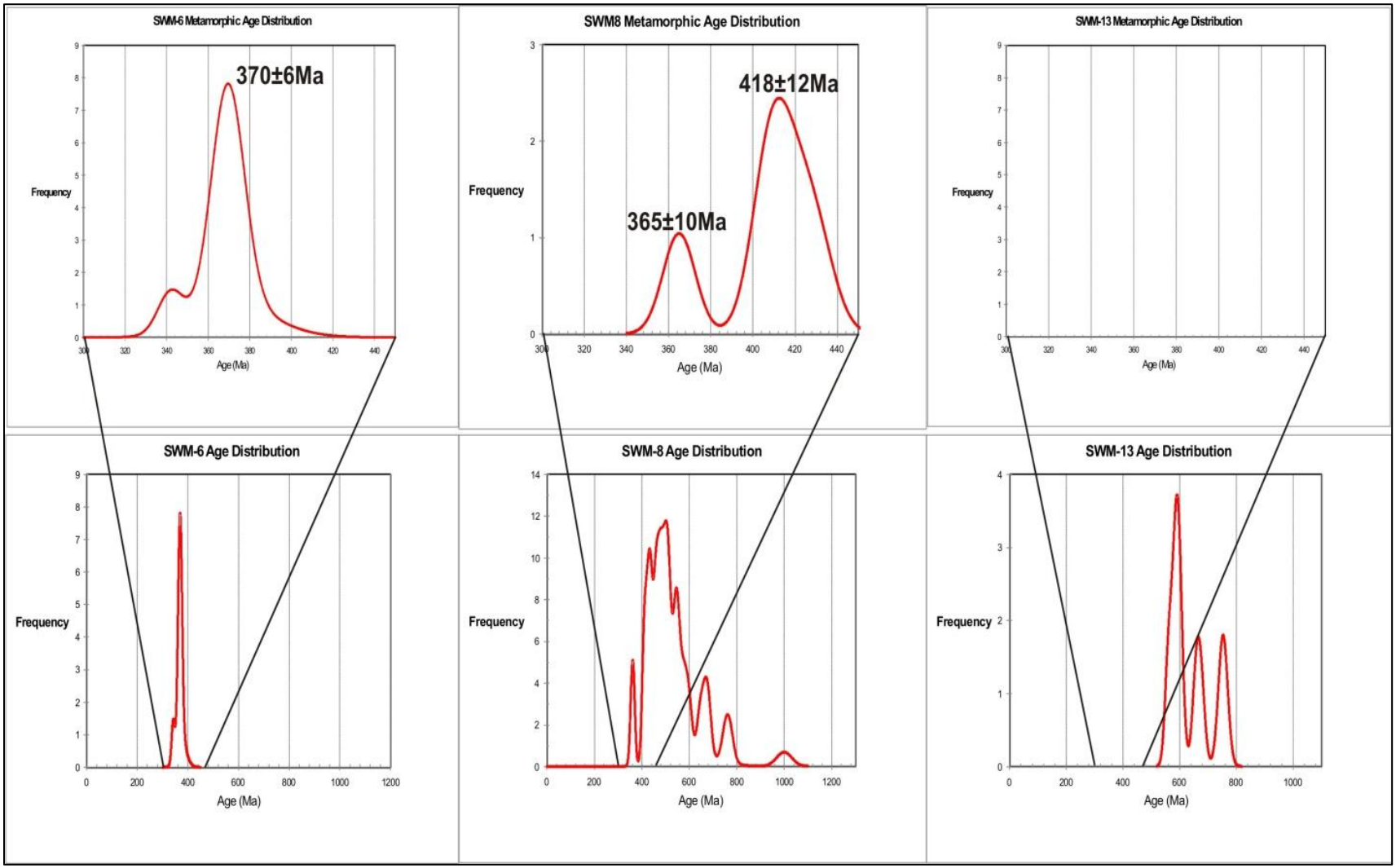

Fig.16: Distribution of age values calculated using concentrations of U-Th-Pb for samples SWM-6, -8 and -13. The White Rock Formation (age) provides the stratigraphic upper boundary of deformation therefore the age values younger than this are interpreted to have Acadian Orogeny origin.

As indicated by this distribution, there exists two age domains preserved in monazite grains from these samples. The first calculated age, which is the older of the two, is preserved within monazites observed in samples SWM-8 and SWM-13. This population ranges from 1000-450 Ma while the second age ranges from 430-360 Ma. The weighted mean age displayed with this distribution was derived using isoplot as follows;

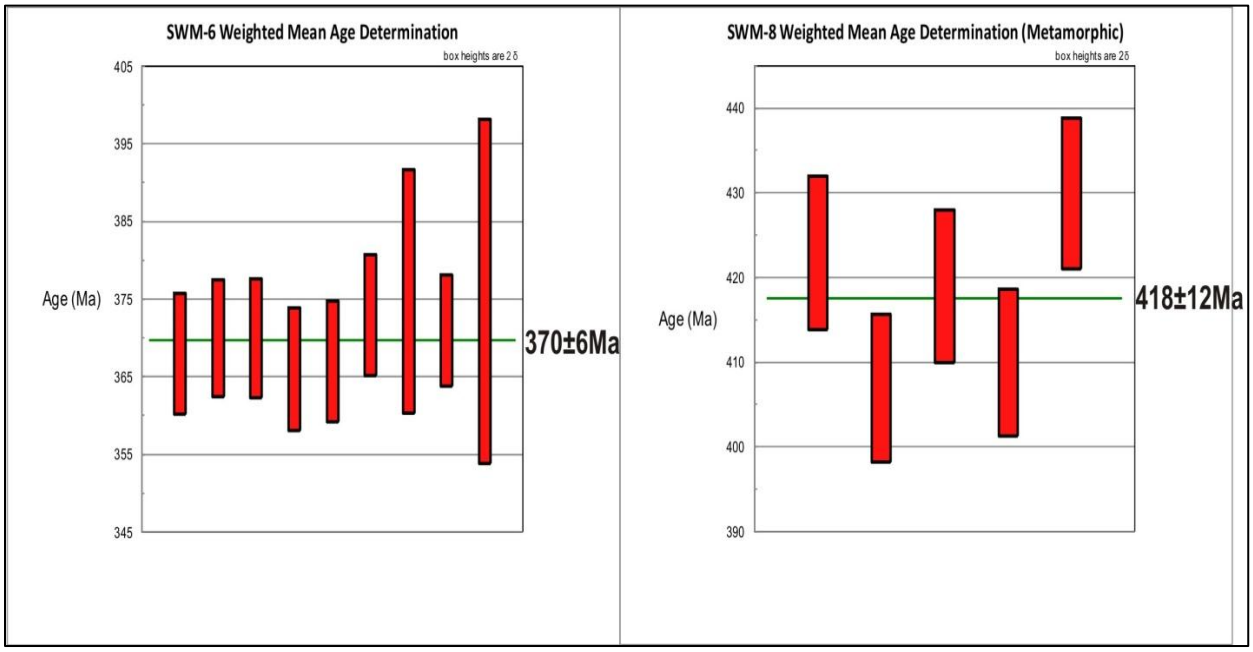

Fig.17: Weighted mean value derived from calculated ages for monazite grains younger than the White Rock Formation in samples SWM-6 and -8.

The distribution is separated in accordance with the age of the White Rock volcanics of southern Nova Scotia. The purpose of this annotation is to indicate the earliest stages of deformation and metamorphism associated with the Acadian Orogeny. Based on this, the interpretation is that any age value older than that of the White Rock Formation represents a detrital monazite while the ages younger than the White Rock Formation would be monazites which formed as a direct result of the metamorphism. The ages calculated for this project appear to coincide with the weighted mean values obtained through zircon U-Th-Pb dating performed

by Waldron et al. (2009). This testing produced a significant peak of age values ranging from 700-600 Ma with minor peaks corresponding Paleozoic and Early-Mid Proterozoic orogenies (Fig.18). As zircon is more resistant to the processes of weathering, these detrital grains are very accurate for the purposes of dating. With the monazite ages being comparable to those of the zircon, it is likely that these detrital grains were from a similar source and represent similar processes of formation.

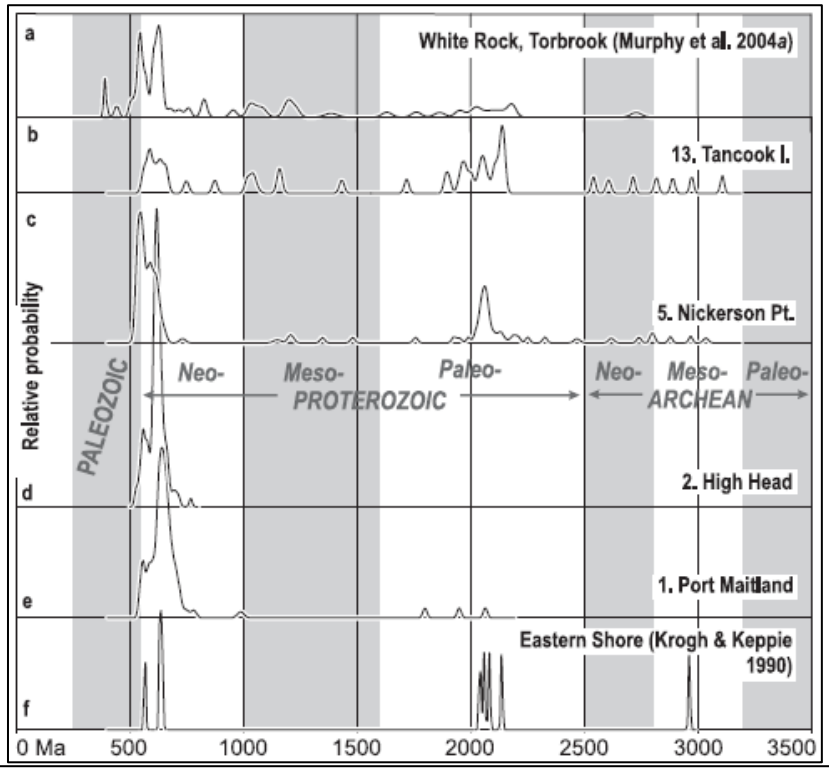

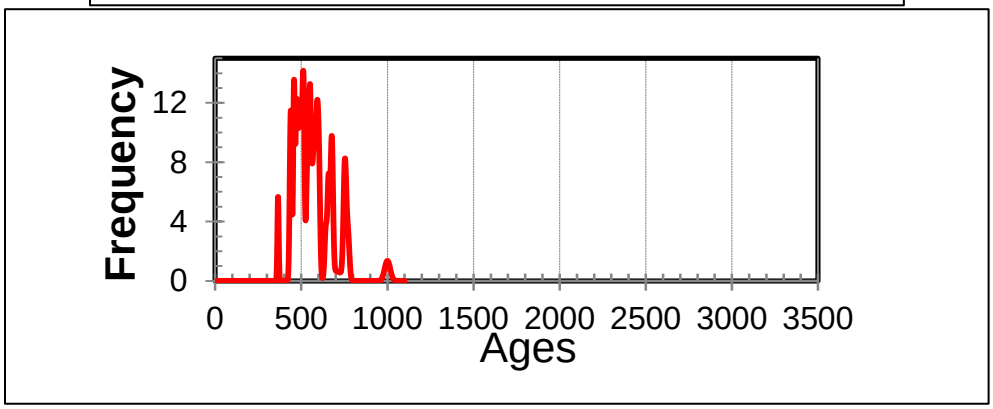

Fig.18: Isoplot detrital zircon age frequency distribution (top) and calculated age of detrital monazites (bottom). Zircon samples collected from various dated fossil locations within the Goldenville Group, Nova Scotia. (Waldron et al., 2009).

5.0 Discussion

5.1 General Statement

Based on the result of the chemical analysis preformed on the monazite grains hosted in samples from southwest Nova Scotia, several key conclusions can be drawn. Firstly, there is a prominent population of monazites which have an age significantly older than that of the Devonian Acadian orogeny. These monazites represent detrital sedimentary grains originally formed from magmatic and metamorphic events associated with the earlier orogenic events which would have affected the region. This contrasts with a separate suite of monazites which yield an age value young enough to be associated with the accepted age of deformation related to the Acadian Orogeny in southern Nova Scotia. These results also provide insight into the metamorphic history of the samples specifically the duration of deformation and temperature conditions subjected to these samples.

5.2 Petrography and Geochronology

These monazite grains are largely represented by the porphyroblast-hosted grains originally interpreted to represent an earlier Acadian-age metamorphic event. The analysis yields a wide spectrum of ages associated with these grains, ranging from 1000-450 Ma. These relatively large monazite grains were deposited along with the passive-margin sediments which originally formed the Halifax and Goldenville Groups. While the older measurements of this suite correspond to the expected ages associated with the early Caledonian and in extreme cases the Grenville orogenies, there are numerous grains which yield ages that do not correlate to

known deformation or intrusion. These anomalous measurements are likely the result of diffusion associated with post-crystallization event(s) and partial resetting of the atomic ratios by mobility of Pb. This occurs due to the conditions of metamorphism that was in cases not of high enough magnitude to grow new monazite grains was capable of influencing the chemical composition of existing grains as well as affecting the euhedral form of the minerals. The resorbed texture which was originally interpreted to represent distinct growth events appears to be an effect of metamorphic overprinting at conditions beneath those which would grow monazite. Larger, resorbed grains supported multiple spot analyses which provide varied age values which illustrate the partial resetting of monazite grains (Fig.19). The monazite grains were in place prior to the growth of biotite and staurolite. The closure temperature of monazite ranges from 800°C down to an upper limit of approx. 600°C while both the observed mineral assemblage and the chemical analysis suggests that the metamorphism which deformed these samples peaked at no greater than 550°C. Because of this, the detrital monazites were not fully reset and therefore retain their original age or a mixed age profile which was derived due to partial diffusion resultant from deformation and increasing thermal conditions. This also contributes to the observed texture of these grains which would have resulted due to the instability of monazite under these changing temperature conditions.

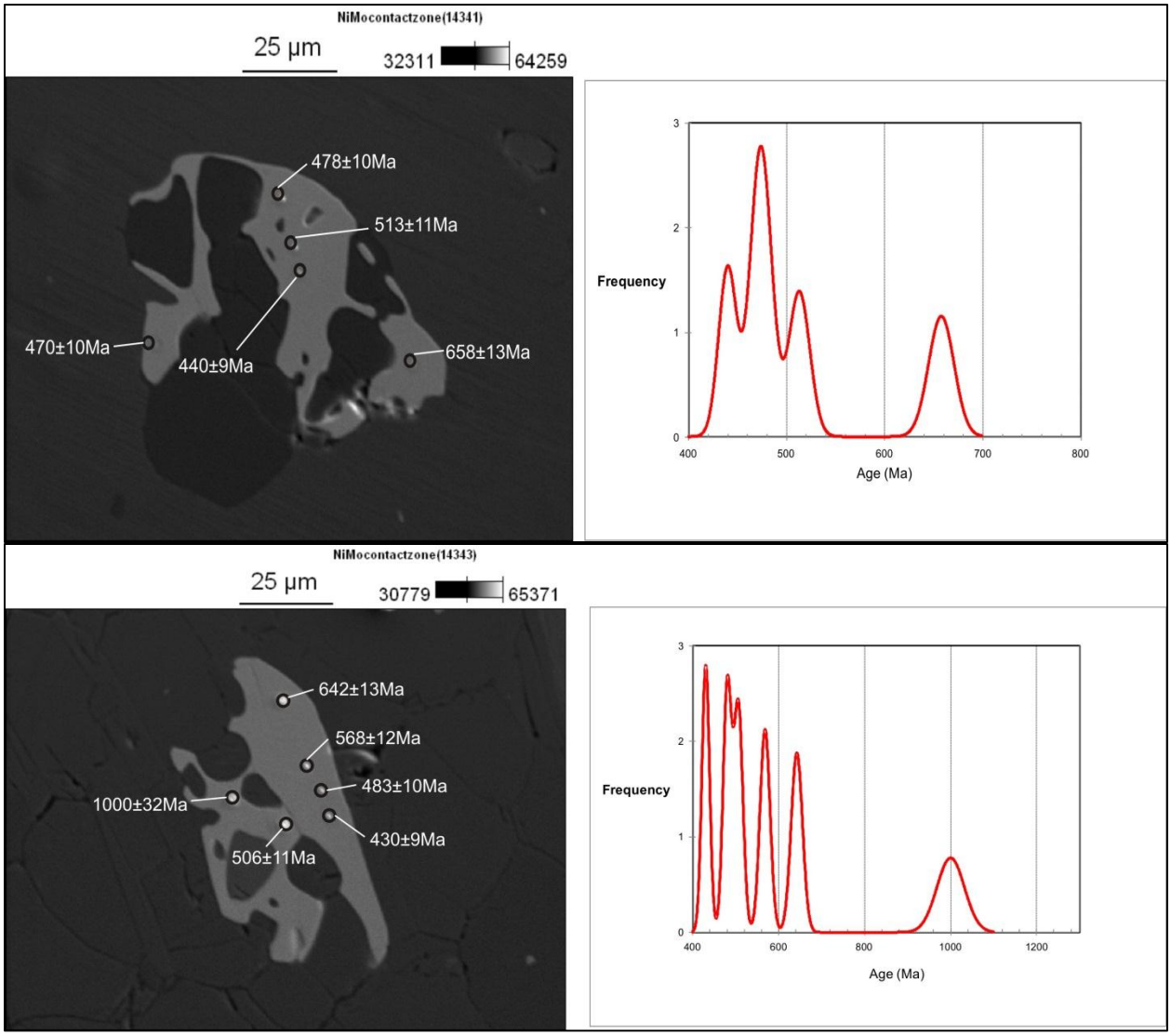

Fig.19: Samples SWM-8 Bt Mnz3 (top) and SWM-8 Mtx Mnz2 (bottom) with annotated spot analysis location and associated calculated age. The varying age is a result of diffusion within the grain during prolonged, low-grade deformation and metamorphism.

The matrix-hosted monazites of sample SWM-6, however, yield younger ages more in line with the ages of the Acadian metamorphic deformation proposed by Hicks et al. (1999). This study used $^{40}Ar/^{39}Ar$ analysis of muscovites of the Lunenburg region of Nova Scotia to determine the age of deformation and produced an age range of 395-388 Ma. This study also produced a suite of muscovite ages representing detrital age grains (600-550 Ma). These detrital muscovite grains display a similar variable reset composition that is observed in the analyzed

monazites indicating the Mahone Bay region samples underwent similar prolonged, low-grade metamorphism. The ages obtained for the monazites identified in sample SWM-6 are more precise than the porphyroblast-hosted samples providing a discrete age range determined to be 370±6 Ma. This age range represents a unique phase of non-detrital, monazite crystallization associated with the Acadian Orogeny. This combined with the euhedral, rutile and quartz aligned form of the analyzed monazite samples is taken as evidence that these grains are metamorphic products and grew as a result of the deformation which also produced the schistosity observed in the samples. This relationship with the matrix indicates that the ages calculated using these minerals represent a relatively high temperature phase of metamorphism. This age is too young to be deformation-related but matches nicely with the ages values associated with post-deformation intrusion. The interpretation of this is that the orogenesis was not of high enough intensity to facilitate the growth of metamorphic monazites and conditions suitable for this were not achieved until the emplacement of granitic plutons in the region.

6.0 Conclusions

6.1 Implications

Due to the textural relationships preserved within the analyzed samples, it appears that the deformed rocks of southern Nova Scotia have undergone a step-wise metamorphic process. This process is identified first by the growth of garnet and biotite porphyroblasts. Following this, the metamorphic conditions increased in magnitude to produce the foliation fabric with the continued growth of later-stage garnet porphyroblasts. With the continued continental collision, staurolite, andalusite and finally cordierite grew at the expense of the previously formed biotite porphyroblasts (as observed by the oscillatory zoning texture of staurolite) due to the effects of contact metamorphism. This prograde metamorphism was followed in turn by retrograde reactions which are most notable in the breakdown of biotite yielding chlorite and the pseudomorphic replacement of staurolite b muscovite.

The focus of this study was to constrain monazite grains which represent these unique metamorphic conditions and use U-Th-Pb dating to determine the timing for the varying stages of crystal growth. Following chemical analysis it was determined that the early monazites represent detrital grains that have been altered under conditions at or moderately below the closure temperature of monazite, thus partially preserving the pre-metamorphic age. The younger, matrix aligned monazites identified in sample SWM-6 yielded a weighted mean age of 370±6 Ma. These grains formed during the granoblastic overprinting associated with contact metamorphism within the samples. Previous work into dating the Acadian Orogeny using foliation-parallel muscovite (samples from the Mahone Bay region, southern Nova Scotia) provided an $^{40}Ar/^{39}Ar$ deformation age range of 395-388 Ma and the high-grade, basement-

extracted monazites of the Popes Harbour dyke yielded U-Pb ages of 378±1 Ma previously reported by Hicks et al. (1999) and Greenough et al. (1999) respectively. The granitic intrusion, specifically the Shelburne Pluton (most proximal to study area), however, has been dated to 372±2Ma which is consistent with the age calculated in this study (Keppie and Krogh, 1999).

Corresponding to this age of monazite crystallization and due to the preservation of the detrital age, it can be concluded that the rocks comprising the Goldenville and Halifax groups within the study area did not reach regional metamorphic conditions significantly greater than 600°C which would be beyond the lower limit of monazite closure temperature but the duration of the metamorphic events was long enough however to facilitate diffusion in many of the detrital grains. The metamorphic age determined in this study constrains the timing of granite emplacement during the Devonian and not the age of deformation associated with the large-scale folding which is observed in the southwest Meguma Terrane.

6.2 Suggestion for Future Work

Based on the analysis of the monazite grains, it is clear that the large, resorbed samples represent detrital grains while the smaller, foliation-parallel monazites were produced by metamorphic deformation. Unfortunately, the large monazites cannot provide information regarding the Acadian Orogeny beyond the textural relationships which they form and as such do not contribute during chemical analysis. Due to this size and textural discrepancy, the smaller metamorphic monazites are more difficult to identify and observe. This limits the ability to constrain the age of specific phases of the stepwise deformation. To gain accuracy in dating these rock samples, it would be advised to increase the number of polished sections produced for samples of the Government Point Formation. This would improve likelihood of observing

monazite grains suitable for obtaining metamorphic ages upon analysis. However, the detrital grains are not without use. There is evidence supporting the theory that the isotopic ratios preserved in the detrital monazites have undergone partial resetting during post-depositional deformation. This diffusion, which occurs at or below the closure temperature of monazite, would provide information regarding the duration of the Acadian Orogeny in southwestern Nova Scotia.

References

Andrehs, G., & Heinrich, W. (1998). Experimental determination of REE distributions between monazite and xenotime: Potential for temperature-calibrated geochronolgy. *Chemical Geology, 149*, 83-96.

Bingen, B., & van Breemen, O. (1998). U-Pb monazite ages in amphibolite- to granulite-facies orthogneiss reflect hydrous mineral breakdown reactions: Sveconorwegian province of SW Norway. *Contributions to Mineralogy and Petrology, 132*, 336-353.

Chu, P. H. (1978). *Metamorphism of the meguma group in the Shelburne area, Nova Scotia* (Unpublished master's thesis). Acadia University.

Cox, R. A. (2003). Morphological, chemical, and geochronological techniques for characterizing detrital zircon. In D. R. Lentz (Ed.), *Geochemistry of sediments and sedimentary rocks: Evolutionary consideration to mineral deposit-forming environments* (pp. 105-120). Toronto, ON: Geological Association of Canada.

Culshaw, N., & Liesa, M. (1997). Alleghanian reactivation of the Acadian Fold Belt, Meguma zone, southwest Nova Scotia. *Canadian Journal of Earth Science, 34*, 833-847.

Culshaw, N., & Reynolds, P. (1997). 40Ar/39Ar age of shear zones in the southwest Meguma zone between Yarmouth and Meteghan, Nova Scotia. *Canadian Journal of Earth Science, 34*, 848-853.

Goldstein, J., Newbury, D., Joy, D., Lyman, C., Echlin, P., Lifshin, E., . . . Michael, J. (2003). *Scanning electron mircoscopy and x-ray analysis* (3rd ed.). New York City: Springer Science.

Greenough, J. D., Krogh, T. E., Kamo, S. L., Owen, J. V., & Ruffman, A. (1999). Precise U-Pb dating of Meguma basement xenoliths: New evidence for Avalonian underthrusting. *Canadian Journal of Earth Science, 36*, 15-22.

Hicks, R., Jamieson, R. A., & Reynolds, P. H. (1999). Detrital and metamorphic 40Ar/39Ar ages from muscovite and whole-rock samples, Meguma Supergroup, southern Nova Scotia. *Canadian Journal of Earth Science, 36*, 23-32.

Kelts, A. B., Ren, M., & Anthony, E. (2008). Monazite occurrence, chemistry, and chronology in the granitoid rocks of the Lachlan Fold Belt, Australia: An electron microprobe study. *American Mineralogist, 93*, 373-383.

Keppie, J. D., & Dallmeyer, R. D. (1995). Late paleozoic collision, delamination, short-lived magmatism, and rapid denudation in the Meguma Terrane (Nova Scotia, Canada): Constraints from 40Ar/39Ar isotopic data. *Canadian Journal of Eath Science, 32*, 644-659.

Keppie, J. D., & Krogh, T. E. (1999). U-Pb geochronology of Devonian granites in the Meguma Terrane of Nova Scotia, Canada: Evidence for hotspot melting of a Neoproterozoic source. *The Journal of Geology, 107*, 555-568.

Kohn, M. J., & Malloy, M. A. (2004). Formation of monazite via prograde metamorphic reactions among common silicates: Implications for age determinations. *Geochimica et Cosmochimca Acta, 68*, 101-113.

Kosler, J. (2008). Laser ablation sampling strategies for concentrations and isotope ratio analysis by ICP-MS. In P. Sylvester (Ed.), *Laser Ablation ICP-MS in the earth sciences: Current practices and outstanding issues* (40th ed., pp. 79-92). Vancouver, BC: Mineralogical Association of Canada.

Linthout, K. (2007). Tripartite division of the system 2REEPO4-CaTh(PO4)2-2ThSiO4, discreditation of brabantite, and recognition of cheralite as the name for members dominated by CaTh(PO4)2. *Canadian Mineralogist, 45*, 503-508.

Lloyd, G. E. (1987). Atomic number and crystallographic contrast images with the SEM: A review of backscattered electron techniques. *Mineralogical Magazine, 51*, 3-19.

Longerich, H. (2008). Laser ablation-inductively coupled plasma-mass spectrometry (LA-ICP-MS); An introduction. In P. Sylvester (Ed.), *Laser-Ablation ICP-MS in earth sciences: Current practises and outstanding issues* (40th ed., pp. 1-18). Vancouver, BC: Mineralogical Association of Canada.

Montel, J.-M., Foret, S., Veschambre, M., Nicollet, C., & Provost, A. (1996). Electron microprobe dating of monazite. *Chemical Geology, 131*, 37-53.

Pan, Y. (1997). Zircon- and monazite-forming metamorphic reations at Manitowadge, Ontario. *Canadian Minerologist, 35*, 105-118.

Parrish, R. R. (1990). U-Pb dating of monazite and its application to geological problems. *Canadian Journal of Earth Science, 27*, 1431-1450.

Pyle, J., Spear, F., Rudnick, R., & McDonough, W. (2001). Monazite-xenotime-garnet equilibrium in metapelites and a new monazite-garnet thermometer. *Journal of Petrology, 42*, 2083-2107.

Rogers, H. D., & Barr, S. M. (1988). Petrology of the Shelburn and Barrington Passage Plutons, southern Nova Scotia. *Maritime Sediments and Atlatic Geology, 24*, 21-31.

Schenk, P. (1997). Sequence stratigraphy and provenance on Gondwana's margin. The Meguma Zone (Cambrian to Devonian) of Nova Scotia, Canada. *GSA Bulletin, 109*, 395-409.

Smith, H. A., & Barreiro, B. (1990). Monazite U-Pb dating of staurolite grade metamorphism in pelitic schists. *Contributions to Mineralogy and Petrology, 105*, 602-615.

Spear, F. S., & Pyle, J. M. (2002). Apatite, monazite and xenotime in metamorphic rocks. *Reviews in Mineralogy and Geochemistry, 48*, 293-335.

Triantafyllidis, S., Pe-Piper, G., MacKay, R., Piper, D. J.W., & Srathdee, G. (2010). *Open File: Vol. 6732. Monazite as a provenance indicator for the Lower Cretaceous reservoir sandstones, Scotian Basin*. Geological Survey of Canada.

Waldron, J., White, C., Barr, S., Simonetti, A., & Heaman, L. (2009). Provenance of the Meguma terrane, Nova Scotia: rifted margin of early Paleozoic Gondwana. *Canadian Journal of Earth Sciences, 46*, 1-8.

White, C. E. (1984). *Structure and metamorphism of the Jordan River Valley, Shelburne County, Nova Scotia* (Unpublished master's thesis). Acadia University.

White, C. E. (2010). Startigraphy of the lower paleozoic Goldenville and Halifax groups in southwestern Nova Scotia. *Atlantic Geology, 46*, 136-154.

Williams, M. L., & Jercinovic, M. J. (2002). Microprobe monazite geochronology: Putting absolute time into microstructral analysis. *Journal of Structural Geology, 24*, 1013-1028.

Williams, M. L., Jercinovic, M. J., Goncalves, P., & Mahan, K. (2006). Format and philosophy for collecting, compiling and reporting microprobe monazite ages. *Chemical Geology, 225*, 1-15.

Williams, M. L., Jercinovic, M. J., & Hetherington, C. J. (2007). Microprobe monazite geochronology: Understanding geologic processes by integrating composition and chronology. *Annual Review of Earth and Planetary Sciences, 35*, 137-175.

Winter, J. D. (2010). *Principles of igneous and metamorphic petrology* (2nd ed.). Upper Saddle River, NJ: Prentice Hall.

Appendix I: Microprobe Data

SWM-6

Comment	P_2O_5	La_2O_3	SiO_2	Pr_2O_3	SO_3	Ce_2O_3	Y_2O_3	Nd_2O_3	PbO	Dy_2O_3	Sm_2O_3	ThO_2	Er_2O_3	Gd_2O_3	UO_2	CaO	Eu_2O_3	Tb_2O_3	Ho_2O_3	Tm_2O_3	Lu_2O_3	Total
SWM 6 pt1	29.351	13.232	0.524	2.844	0.042	25.271	1.894	11.508	0.303	0.853	2.057	4.963	0	1.675	0.656	1.056	0.909	0.12	0.134	0.212	0.034	97.638
SWM 6 pt2	30.03	14.598	0.501	2.795	0.101	28.028	1.508	11.95	0.186	0.624	2.079	3.14	0	1.256	0.506	0.714	0.961	0.087	0	0.296	0.08	99.44
SWM 6 pt3	30.097	15.008	0.074	3.121	0	28.621	1.285	13.154	0.083	0.619	2.15	2.291	0	1.428	0.252	0.448	1.102	0.131	0	0.321	0.12	100.31
SWM 6 pt4	29.605	12.91	0.493	2.447	0	25.094	2.008	11.291	0.239	0.863	1.947	6.328	0.049	1.85	0.753	1.299	0.879	0.221	0.163	0.225	0.108	98.772
SWM 6 pt5	29.106	12.705	0.29	2.501	0.102	24.436	1.881	11.303	0.064	0.803	2.069	7.384	0	1.802	0.7	1.482	0.9	0.157	0.208	0.224	0.076	98.193
SWM 6 pt6	29.157	13.799	0.593	2.626	0	27.483	0.6	12.253	0.255	0.362	2.297	5.054	0	1.635	0.613	1.004	0.855	0	0.021	0.23	0.055	98.892
SWM 6 pt7	29.529	13.379	0.392	2.732	0.033	26.327	1.449	11.495	0.332	0.655	2.296	7.434	0	1.723	0.438	1.363	0.89	0	0.118	0.255	0.072	100.91
SWM 6 pt8	29.055	13.274	0.921	2.875	0.006	26.436	0	11.425	0.304	0	1.897	9.697	0	0.998	0.474	1.556	0.757	0	0	0.237	0	99.912
SWM 6 pt9	29.327	14.016	0.556	3.005	0.003	27.54	0.191	12.573	0.226	0	2.093	5.565	0	1.28	0.618	1.074	0.802	0	0	0.222	0	99.091
SWM 6 pt10	24.463	10.075	0.509	2.017	0	19.873	0.621	9.056	0.022	0.279	1.523	2.639	0.046	0.758	0.267	0.467	0.707	0	0	0.209	0.082	73.613
SWM 6 pt11	29.629	14.081	0.17	2.715	0.015	28.208	1.431	13.19	0.197	0.412	2.163	2.72	0	1.52	0.333	0.59	1.124	0	0	0.15	0.048	98.696
SWM 6 pt12	29.172	14.172	0.27	2.883	0.079	28.42	1.351	12.465	0.231	0.4	1.839	2.554	0.025	1.359	0.44	0.595	1.157	0	0	0.12	0.018	97.55
SWM 6 pt13	29.139	14.199	0.009	2.787	0	27.495	1.58	12.169	0.175	0.422	2.044	2.806	0	1.574	0.493	0.644	1.035	0	0	0.174	0.084	96.829
SWM 6 pt14	29.385	13.696	0.001	2.748	0.031	26.52	1.978	12.395	0.187	0.446	2.347	3.198	0	1.643	0.629	0.757	1.064	0	0	0.262	0.065	97.352
SWM 6 pt15	28.014	13.476	0.107	2.52	0.012	26.443	1.851	11.942	0.309	0.751	2.359	5.035	0	1.959	0.736	1.092	0.969	0	0.17	0.235	0.072	98.052
SWM 6 pt16	28.613	14.259	0.171	2.838	0.067	28.033	0.734	12.395	0.042	0.265	2.192	3.667	0	1.228	0.534	0.858	1.008	0	0	0.282	0.154	97.34
SWM 6 pt17	27.854	14.208	0.108	3.002	0	28.177	1.476	12.552	0.227	0.704	1.903	2.376	0	1.499	0.415	0.615	1.048	0.141	0	0.287	0.104	96.696

SWM 6 pt18	27.77	14.267	0.281	3.091	0	28.252	0.571	12.973	0.139	0.254	2.193	3.959	0	1.583	0.329	0.826	0.815	0.139	0	0.192	0.027	97.661
SWM 6 pt19	27.456	13.596	0.435	2.599	0.023	26.383	0.178	12.061	0.144	0	2.068	7.556	0	1.224	0.768	1.504	0.821	0	0	0.067	0.068	96.951
SWM 6 pt20	27.746	14.655	0.009	2.877	0	28.279	1.529	12.332	0.122	0.568	2.103	2.411	0	1.461	0.54	0.633	0.99	0	0	0.229	0.159	96.643
SWM 6 pt21	30.765	14.326	0.039	2.818	0	28.537	1.602	12.655	0.106	0.792	2.163	2.541	0.016	1.708	0.491	0.6	1.022	0.209	0	0.292	0	100.68
SWM 6 pt22	29.992	14.412	0.225	3.057	0	28.823	0.764	12.526	0.192	0.477	2.024	2.511	0	1.223	0.392	0.616	1.009	0.102	0	0.225	0.087	98.657
SWM 6 pt23	29.482	14.156	0.429	3.15	0.039	27.222	1.685	12.743	0.07	0.445	2.205	2.27	0	1.527	0.532	0.579	1.039	0.118	0.007	0.302	0.01	98.01
SWM 6 pt24	30.031	14.838	0	3.257	0	28.142	1.376	12.943	0.188	0.679	2.103	1.782	0	1.566	0.461	0.449	1.049	0.135	0.036	0.17	0	99.205
SWM 6 pt25	30.671	14.267	0	2.824	0.014	26.918	2.307	13.892	0.277	0.525	2.932	0.606	0.054	1.938	0.336	0.362	1.039	0.075	0.026	0.409	0.13	99.602
SWM 6 pt26	30.672	13.507	0.021	2.931	0.01	27.62	1.535	14.711	0.004	0.355	2.705	0.776	0	1.516	0.499	0.675	1.075	0	0	0.342	0.062	99.016
SWM 6 pt28	30.018	14.418	0.022	2.891	0.012	28.198	1.58	13.659	0.168	0.586	2.398	0.614	0	1.632	0.366	0.315	1.228	0.028	0	0.318	0.069	98.52
SWM 6 pt29	30.48	14.68	0	2.881	0.02	28.051	1.525	13.388	0.091	0.078	2.402	1.071	0	1.404	0.431	0.397	1.072	0	0	0.287	0.08	98.338
SWM 6 pt30	29.213	13.841	0.894	2.684	0.007	27.618	1.381	13.279	0.106	0	2.208	1.31	0	1.629	0.422	0.539	1.012	0	0	0.22	0.008	96.371
SWM 6 pt31	29.938	14.6	0.132	2.878	0	28.867	1.348	13.231	0.104	0.456	2.257	1.439	0.039	1.351	0.436	0.404	1.126	0.003	0	0.259	0	98.868
SWM 6 pt32	29.54	14.002	0	2.911	0.055	26.954	1.838	12.638	0.119	0.397	2.157	1.528	0.041	1.476	1.223	0.619	0.989	0	0	0.323	0.05	96.86
SWM 6 pt33	30.158	12.495	0	2.833	0.011	26.037	2.733	12.993	0.15	0.894	2.683	2.867	0.058	1.896	0.864	0.797	1.031	0	0.154	0.279	0.126	99.059
SWM 6 pt34	28.581	13.93	0.275	2.749	0.076	27.214	1.015	12.857	0.18	0	2.111	3.165	0	1.413	0.372	0.762	0.966	0	0	0	0	95.666
SWM 6 pt35	29.352	14.06	0.264	2.785	0	27.47	0.602	12.635	0.228	0.256	2.088	4.429	0	1.474	0.432	0.932	1.059	0	0	0.236	0.02	98.322
SWM 6pt36	29.291	14.444	0.082	2.864	0.039	28.535	1.108	12.606	0.071	0.523	2.015	2.624	0	1.453	0.401	0.586	1.054	0	0	0.138	0.083	97.917

SWM-13																						
Comment	**P_2O_5**	**La_2O_3**	**SiO_2**	**Pr_2O_3**	**SO_3**	**Ce_2O_3**	**Y_2O_3**	**Nd_2O_3**	**PbO**	**Dy_2O_3**	**Sm_2O_3**	**ThO_2**	**Er_2O_3**	**Gd_2O_3**	**UO_2**	**CaO**	**Eu_2O_3**	**Tb_2O_3**	**Ho_2O_3**	**Tm_2O_3**	**Lu_2O_3**	**Total**
SWM 13 Mnz1 pt 1	29.583	13.196	0.133	2.719	0.071	27.376	1.49	12.598	0.021	0.702	2.095	5.16	0	1.535	0.449	1.061	1.147	0.19	0	0.292	0.078	99.896
SWM 13 pt 2	30.372	13.207	0.105	2.649	0.158	26.461	1.612	11.757	0.167	0.767	2.039	6.315	0.025	1.622	0.427	1.211	1.037	0.165	0.024	0.243	0.019	100.38
SWM 13 pt 3	29.235	12.227	0.188	2.624	0.131	25.204	1.628	11.536	0.263	0.84	1.947	7.204	0	1.489	0.579	1.403	1.059	0.153	0.081	0.276	0.002	98.069
SWM 13 pt 4	29.595	13.078	0.148	2.697	0.087	26.853	1.463	11.765	0.164	0.672	1.922	6.081	0.021	1.44	0.405	1.197	1.145	0.125	0.002	0.28	0.017	99.157
SWM 13 pt 5	29.491	12.671	0.155	2.66	0.075	26.869	1.557	12.133	0.035	0.751	2.069	5.615	0	1.63	0.275	1.106	1.114	0.21	0	0.229	0.017	98.662
swm 13 pt 6 (Mnz2)	29.846	13.251	0.119	2.887	0.061	27.066	1.52	12.203	0.17	0.684	1.899	4.45	0.035	1.586	0.47	0.954	1.005	0.167	0	0.23	0.069	98.672
swm 13 pt 7	29.23	12.073	0.314	2.43	0.083	23.365	1.769	11.102	0.386	0.866	1.998	9.424	0	1.781	0.631	1.772	0.872	0.251	0.086	0.243	0.02	98.696
swm 13 pt 8	29.952	12.978	0.065	2.879	0.03	26.978	1.528	12.239	0.237	0.709	2.232	4.95	0	1.669	0.383	0.967	1.068	0.17	0	0.254	0.064	99.352
swm 13 pt 9	29.777	12.992	0.164	2.724	0.054	26.713	1.667	12.307	0.124	0.846	1.968	5.548	0	1.681	0.336	1.127	1.089	0.246	0	0.249	0.028	99.64
swm 13 pt 10	28.555	12.619	0.239	2.763	0.143	26.472	1.611	11.767	0.239	0.824	2.027	5.392	0	1.55	0.384	1.103	1.068	0.122	0	0.203	0.002	97.083
SWM 13 pt 11 (Mnz3)	29.32	13.041	0.111	2.546	0.054	25.954	1.591	11.493	0.261	0.732	1.882	6.141	0	1.513	0.516	1.312	0.994	0.105	0	0.26	0.07	97.896
SWM 13 pt 12	29.868	12.78	0.118	2.732	0.106	27.388	1.448	12.31	0.253	0.747	2.001	4.348	0	1.536	0.395	0.875	1.142	0.172	0	0.204	0.094	98.517
SWM 13 pt 13	30.034	13.915	0.079	2.602	0.086	27.363	1.505	11.917	0.17	0.865	2.007	4.62	0	1.359	0.409	0.978	1.063	0.064	0	0.241	0.099	99.376
SWM 13 pt 14	28.445	12.134	0.225	2.699	0.045	25.486	1.673	11.6	0.126	0.726	2.066	6.971	0.021	1.702	0.579	1.361	1.06	0.121	0	0.227	0.041	97.308
SWM 13 pt 15 (Mnz4)	30.074	12.97	0.091	2.626	0.09	27.465	1.687	12.579	0.142	0.819	2.273	3.029	0	1.928	0.562	0.778	1.07	0.159	0	0.276	0.107	98.725
swm 13 pt 16	30.26	13.412	0.147	2.866	0.069	27.944	1.547	12.295	0.169	0.881	2.028	3.264	0.238	1.806	0.427	0.817	1.169	0.176	0	0.295	0.111	99.921
swm 13 pt 17	29.081	13.498	0.097	2.752	0.047	28.053	1.461	12.475	0.094	1.057	2.129	2.6	0	1.666	0.336	0.639	1.111	0.217	0	0.274	0.126	97.713
SWM 13 pt 18 (Mnz5)	29.258	13.408	0.046	2.611	0.104	26.599	1.649	12.264	0.239	0.885	2.044	3.469	0	1.58	0.556	0.856	1.082	0.141	0	0.226	0.103	97.12
swm 13 pt 19	29.249	15.361	0.098	2.622	0.181	28.005	1.372	11.236	0.064	0.551	1.848	2.768	0	1.219	0.479	0.939	0.91	0.132	0	0.259	0.052	97.345
swm 13 pt 20	29.218	13.843	0.092	2.832	0.14	27.5	1.469	12.698	0.182	0.733	2.147	3.041	0	1.626	0.365	0.741	1.082	0.185	0	0.229	0.026	98.149

SWM-8																						
Comment	**P_2O_5**	**La_2O_3**	**SiO_2**	**Pr_2O_3**	**SO_3**	**Ce_2O_3**	**Y_2O_3**	**Nd_2O_3**	**PbO**	**Dy_2O_3**	**Sm_2O_3**	**ThO_2**	**Er_2O_3**	**Gd_2O_3**	**UO_2**	**CaO**	**Eu_2O_3**	**Tb_2O_3**	**Ho_2O_3**	**Tm_2O_3**	**Lu_2O_3**	**Total**
SWM8 Mtx mnz 1 pt1	29.165	14.645	0	3.114	0.025	29.559	1.425	12.97		0.561	2.162	1.903	0	1.694	0.149	0.507	0.997	0	0	0.245	0.065	99.186
pt 2	29.21	14.5	0	3.345	0	29.808	1.43	13.177		0.646	2.333	1.442	0.177	1.754	0.294	0.38	1.124	0.135	0	0.322	0.052	100.13
pt 3	29.273	14.791	0	3.258	0.04	30.231	1.473	12.777		0.496	1.902	1.159	0	1.4	0.219	0.39	0.999	0.061	0	0.311	0.084	98.864
pt 4	28.83	12.772	0.092	2.982	0.002	26.762	1.316	12.383		0.799	2.506	5.918	0	1.947	0.448	1.2	0.943	0.144	0.173	0.293	0.049	99.559
pt 5	29.713	14.148	0	3.038	0.001	27.955	1.671	12.363		0.713	2.326	3.389	0	1.884	0.15	0.778	1.037	0.153	0	0.28	0	99.599
SWM8 Bt mnz 1 pt 1	29.594	14.536	0	3.067	0	29.725	1.546	12.865		0.484	2.214	1.799	0	1.62	0.267	0.463	1.022	0	0	0.218	0.053	99.473
pt 2	29.547	14.437	0	3.105	0.029	29.184	1.439	13.048		0.565	2.349	1.738	0	1.65	0.169	0.422	0.967	0	0	0.121	0.04	98.81
pt 3	29.427	13.774	0	3.031	0.006	27.895	1.767	13.037		0.702	2.372	2.485	0	2.016	0.305	0.648	1.059	0	0.007	0.32	0.063	98.914
pt 4	30.336	14.194	0	3.195	0.018	29.591	1.611	13.213		0.664	2.341	1.981	0.038	2.001	0.275	0.517	1.047	0.026	0.021	0.274	0.045	101.39
pt 5	29.478	14.261	0	3.075	0.001	28.191	1.606	13.003		0.579	2.57	2.688	0.032	2.28	0.315	0.651	1.01	0.01	0.033	0.274	0.079	100.14
SMW8 bt mnz 2 pt1	28.325	12.506	0.164	2.77	0	25.704	1.184	11.767		0.456	2.411	7.884	0	1.986	0.425	1.513	0.857	0	0.063	0.27	0	98.285
pt 2	29.103	14.09	0	3.045	0.005	28.743	1.591	12.584		0.53	2.107	2.554	0	1.645	0.323	0.584	0.963	0	0	0.177	0.128	98.172
pt 3	29.325	14.956	0	3.124	0.043	29.596	1.319	12.62		0.401	1.951	1.497	0	1.461	0.149	0.405	1.075	0	0	0.213	0.047	98.182
pt 4	29.461	12.958	0	2.856	0	26.885	1.902	12.36		0.634	2.404	4.058	0.038	1.995	0.439	0.953	0.945	0	0.187	0.332	0.034	98.441
pt 5	28.52	13.519	0.159	3.044	0	27.16	1.696	11.955		0.507	2.268	2.821	0	1.94	0.312	0.915	1.038	0	0.127	0.252	0.031	96.264
SMW8 Mtx mnz2 pt 1	29.665	14.83	0	3.283	0.01	29.542	1.525	12.891		0.713	2.319	2.012	0	1.669	0.296	0.513	1.046	0.182	0	0.269	0	100.77
pt 2	29.133	12.796	0	2.704	0	26.327	1.618	12.154		0.875	2.468	6.287	0	2.111	0.605	1.425	0.925	0.212	0.244	0.283	0.128	100.3
pt 3	29.469	13.167	0	2.903	0	26.924	2.06	12.25		1.006	2.419	4.711	0	2.084	0.548	1.104	1.035	0.137	0.218	0.25	0.04	100.33
pt 4	29.438	12.738	0	2.846	0.046	26.344	2.09	12.07		0.92	2.365	5.134	0	2.173	0.572	1.228	0.94	0.235	0.216	0.308	0.045	99.708
pt 5	29.244	12.812	0.189	2.727	0.047	25.909	0.337	12.588		0.357	2.224	8.387	0	1.614	0.734	2.008	0.754	0.196	0	0.225	0.073	100.43
pt 6	29.008	13.467	0.131	2.998	0.05	28.186	0.499	12.95		0.297	2.333	5.724	0	1.711	0.212	1.292	0.866	0.092	0	0.198	0.056	100.07
SMW8 Mtx mnz3 pt1	29.267	14.01	0.117	3.095	0.034	28.837	0.442	12.608		0.256	2.265	4.296	0.07	1.529	0.283	1.05	0.804	0	0	0.274	0	99.237
pt2	28.514	13.583	0.336	2.814	0.058	26.128	0	11.331		0.041	1.856	10.112	0.034	0.766	0.278	1.756	0.767	0.075	0	0.124	0.045	98.618

pt3	29.306	13.961	0.175	3.231	0	28.077	0.123	12.891		0.181	2.013	5.244	0	1.375	0.281	1.105	0.933	0.106	0	0.229	0	99.231
pt4	28.534	12.719	0.296	2.662	0.004	25.749	0.03	11.212		0.171	1.876	10.937	0	1.097	0.381	2.029	0.761	0	0	0.229	0.054	98.741
pt5	29.589	13.586	0.047	3.108	0.029	28.381	1.377	13.039		0.713	2.545	2.482	0	1.875	0.166	0.546	0.983	0.076	0.069	0.293	0.125	99.029
pt6	29.574	13.925	0	3.073	0	28.946	1.267	12.732		0.503	2.15	2.841	0	1.537	0.322	0.713	1.03	0.074	0	0.325	0.038	99.05
pt7	30.137	13.146	0	3.054	0.013	27.845	1.94	12.592		0.787	2.227	2.887	0	1.875	0.238	0.708	1.002	0.082	0.116	0.252	0.028	98.929
smw8 bt mnz3 pt1	29.817	13.453	0	3.072	0	27.396	1.974	12.208		0.744	2.269	3.712	0	1.9	0.524	0.879	0.981	0	0.145	0.264	0.062	99.4
pt2	29.413	15.362	0.117	3.189	0.026	30.394	0.07	13.124		0	2.096	3.407	0.002	1.324	0.302	0.861	0.891	0	0	0.232	0.054	100.86
pt3	29.058	14.743	0.134	3.147	0.01	28.173	0.01	12.335		0.071	1.894	6.072	0	1.287	0.308	1.218	0.86	0	0	0.257	0.008	99.585
pt4	28.653	12.365	0.303	2.787	0.047	25.678	0	11.467		0.124	1.846	10.356	0	1.204	0.621	2.098	0.779	0	0	0.172	0.114	98.614
pt5	29.88	14.781	0	3.23	0.018	28.225	1.88	12.418		0.529	2.244	2.108	0	1.765	0.46	0.571	1.025	0	0	0.177	0.104	99.415
SMW8 bt mnz4 pt1	29.275	14.161	0.097	3.087	0.047	28.379	0.668	12.944		0.404	2.376	3.294	0	1.9	0.401	0.769	0.932	0	0	0.274	0	99.008
pt2	29.54	13.781	0	3.076	0.009	28.264	1.4	13.041		0.624	2.431	2.98	0	2.065	0.318	0.673	1.01	0.073	0	0.218	0.025	99.528
SWM-?? mnzinstau-1 pt1	29.229	14.301	0	3.227	0.069	27.78	1.583	12.161		0.302	1.853	3.059	0	1.464	0.457	0.652	1.036	0	0	0.096	0.072	97.341
SWM-?? mnzinstau-1 pt2	29.505	14.846	0.023	3.292	0.03	28.822	1.407	12.418		0.169	1.969	1.786	0	1.451	0.489	0.422	1.15	0	0	0.199	0.07	98.048
swm-?? sta-mnz2 pt1	29.15	14.303	0.034	3.049	0.031	27.608	1.497	11.899		0.214	1.945	3.759	0	1.243	0.508	0.812	1.062	0	0	0.19	0.098	97.402
swm-?? sta-mnz2 pt2	29.44	14.107	0.054	3.073	0	26.789	1.488	11.534		0.485	2.021	4.577	0	1.497	0.289	0.929	1.064	0	0	0.174	0.03	97.551
swm-?? sta-mnz2 pt3	29.55	14.764	0	2.974	0.02	28.25	1.572	11.793		0.463	1.995	2.628	0	1.456	0.327	0.682	1.075	0	0	0.174	0.104	97.827
swm-?? sta-mnz2 pt4	28.98	13.982	0.023	3.134	0.059	27.134	1.636	12.018		0.402	1.972	3.305	0	1.432	0.342	0.844	0.913	0	0	0.156	0	96.332

(mass %)

	Th	U	Y	Pb	P	La	Si	Pr	Ca	Ce	Nd	Dy	Sm	Gd	O	Total
SWM 8 Mtx Mnz2 pt1	1.568	0.195	0.727	0.064	12.5	11.87	0.13	2.36	0.73	23.09	10.42	0.46	1.85	1.37	27.07	94.404
SWM 8 Mtx Mnz2 pt2	2.733	0.3	0.734	0.095	12.5	11.87	0.13	2.36	0.73	23.09	10.42	0.46	1.85	1.37	27.07	95.712
SWM 8 Mtx Mnz2 pt3	4.494	0.715	0.667	0.147	12.5	11.87	0.13	2.36	0.73	23.09	10.42	0.46	1.85	1.37	27.07	97.873
SWM 8 Mtx Mnz2 pt4	4.626	0.619	0.975	0.128	12.5	11.87	0.13	2.36	0.73	23.09	10.42	0.46	1.85	1.37	27.07	98.198
SWM 8 Mtx Mnz2 pt5	1.874	0.253	0.54	0.232	12.5	11.87	0.13	2.36	0.73	23.09	10.42	0.46	1.85	1.37	27.07	94.749
SWM 8 Mtx Mnz2 pt6	4.528	0.378	0.154	0.131	12.5	11.87	0.13	2.36	0.73	23.09	10.42	0.46	1.85	1.37	27.07	97.041
SWM 8 Mtx Mnz3 pt1	4.106	0.3	0.208	0.118	12.5	11.87	0.13	2.36	0.73	23.09	10.42	0.46	1.85	1.37	27.07	96.582
SWM 8 Mtx Mnz3 pt2	6.793	0.327	0.009	0.188	12.5	11.87	0.13	2.36	0.73	23.09	10.42	0.46	1.85	1.37	27.07	99.167
SWM 8 Mtx Mnz3 pt3	5.166	0.343	0.21	0.139	12.5	11.87	0.13	2.36	0.73	23.09	10.42	0.46	1.85	1.37	27.07	97.708
SWM 8 Mtx Mnz3 pt4	8.632	0.491	0.072	0.199	12.5	11.87	0.13	2.36	0.73	23.09	10.42	0.46	1.85	1.37	27.07	101.244
SWM 8 Mtx Mnz3 pt5	4.21	0.347	0.456	0.123	12.5	11.87	0.13	2.36	0.73	23.09	10.42	0.46	1.85	1.37	27.07	96.986
SWM 8 Mtx Mnz3 pt6	3.266	0.46	0.925	0.106	12.5	11.87	0.13	2.36	0.73	23.09	10.42	0.46	1.85	1.37	27.07	96.607
SWM 8 Bt Mnz1 pt1	1.783	0.211	0.776	0.076	12.5	11.87	0.13	2.36	0.73	23.09	10.42	0.46	1.85	1.37	27.07	94.696
SWM 8 Bt Mnz1 pt2	2.087	0.238	0.814	0.059	12.5	11.87	0.13	2.36	0.73	23.09	10.42	0.46	1.85	1.37	27.07	95.048
SWM 8 Bt Mnz1 pt3	3.008	0.286	0.805	0.078	12.5	11.87	0.13	2.36	0.73	23.09	10.42	0.46	1.85	1.37	27.07	96.027
SWM 8 Bt Mnz1 pt4	3.693	0.32	0.709	0.117	12.5	11.87	0.13	2.36	0.73	23.09	10.42	0.46	1.85	1.37	27.07	96.689
SWM 8 Bt Mnz1 pt5	1.464	0.205	0.708	0.075	12.5	11.87	0.13	2.36	0.73	23.09	10.42	0.46	1.85	1.37	27.07	94.302
SWM 8 Bt Mnz2 pt1	4.435	0.438	0.371	0.124	12.5	11.87	0.13	2.36	0.73	23.09	10.42	0.46	1.85	1.37	27.07	97.218
SWM 8 Bt Mnz2 pt2	3.316	0.279	0.804	0.069	12.5	11.87	0.13	2.36	0.73	23.09	10.42	0.46	1.85	1.37	27.07	96.318
SWM 8 Bt Mnz2 pt3	1.286	0.177	0.687	0.042	12.5	11.87	0.13	2.36	0.73	23.09	10.42	0.46	1.85	1.37	27.07	94.042
SWM 8 Bt Mnz2 pt4	1.928	0.212	0.804	0.065	12.5	11.87	0.13	2.36	0.73	23.09	10.42	0.46	1.85	1.37	27.07	94.859
SWM 8 Bt Mnz2 pt5	2.149	0.292	0.697	0.075	12.5	11.87	0.13	2.36	0.73	23.09	10.42	0.46	1.85	1.37	27.07	95.063
SWM 8 Bt Mnz3 pt1	3.123	0.382	0.7	0.092	12.5	11.87	0.13	2.36	0.73	23.09	10.42	0.46	1.85	1.37	27.07	96.147
SWM 8 Bt Mnz3 pt2	5.049	0.362	0.032	0.135	12.5	11.87	0.13	2.36	0.73	23.09	10.42	0.46	1.85	1.37	27.07	97.428
SWM 8 Bt Mnz3 pt3	5.515	0.412	0.057	0.158	12.5	11.87	0.13	2.36	0.73	23.09	10.42	0.46	1.85	1.37	27.07	97.992
SWM 8 Bt Mnz3 pt4	4.338	0.33	0.124	0.107	12.5	11.87	0.13	2.36	0.73	23.09	10.42	0.46	1.85	1.37	27.07	96.749
SWM 8 Bt Mnz3 pt5	1.387	0.334	0.796	0.074	12.5	11.87	0.13	2.36	0.73	23.09	10.42	0.46	1.85	1.37	27.07	94.441
SWM 8 Bt Mnz4 pt1	3.035	0.278	0.304	0.101	12.5	11.87	0.13	2.36	0.73	23.09	10.42	0.46	1.85	1.37	27.07	95.568
SWM 8 Bt Mnz4 pt2	2.396	0.262	0.692	0.079	12.5	11.87	0.13	2.36	0.73	23.09	10.42	0.46	1.85	1.37	27.07	95.279
SWM 8 Bt Mnz4 pt3	1.756	0.189	0.62	0.092	12.5	11.87	0.13	2.36	0.73	23.09	10.42	0.46	1.85	1.37	27.07	94.507

SWM 8 matrix mnz 1	1.441	0.175	1.156	0.057	12.5	11.87	0.13	2.36	0.73	23.09	10.42	0.46	1.85	1.37	27.07	94.679
SWM 8 matrix mnz 2	2.138	0.215	1.134	0.063	12.5	11.87	0.13	2.36	0.73	23.09	10.42	0.46	1.85	1.37	27.07	95.4
SWM 8 matrix mnz 3	1.602	0.191	1.228	0.054	12.5	11.87	0.13	2.36	0.73	23.09	10.42	0.46	1.85	1.37	27.07	94.925
SWM 8 matrix mnz 4	2.394	0.239	1.058	0.082	12.5	11.87	0.13	2.36	0.73	23.09	10.42	0.46	1.85	1.37	27.07	95.623
SWM 8 matrix mnz 5	2.469	0.278	1.25	0.071	12.5	11.87	0.13	2.36	0.73	23.09	10.42	0.46	1.85	1.37	27.07	95.918
SWM 8 matrix mnz 6	7.812	0.366	0.996	0.169	12.5	11.87	0.13	2.36	0.73	23.09	10.42	0.46	1.85	1.37	27.07	101.193
SWM 8 matrx mnz 7	5.832	0.534	1.509	0.146	12.5	11.87	0.13	2.36	0.73	23.09	10.42	0.46	1.85	1.37	27.07	99.871
SWM 8 matrx mnz 8	6.454	0.382	0.812	0.12	12.5	11.87	0.13	2.36	0.73	23.09	10.42	0.46	1.85	1.37	27.07	99.618
SWM 8 matrx mnz 9	2.816	0.298	0.985	0.083	12.5	11.87	0.13	2.36	0.73	23.09	10.42	0.46	1.85	1.37	27.07	96.032
SWM 8 matrx mnz 10	3.095	0.281	1.206	0.082	12.5	11.87	0.13	2.36	0.73	23.09	10.42	0.46	1.85	1.37	27.07	96.514
SWM 8 matrx mnz 11	2.628	0.329	0.939	0.076	12.5	11.87	0.13	2.36	0.73	23.09	10.42	0.46	1.85	1.37	27.07	95.822
SWM 8 matrx mnz 12	2.725	0.297	1.245	0.07	12.5	11.87	0.13	2.36	0.73	23.09	10.42	0.46	1.85	1.37	27.07	96.187
SWM 8 matrx mnz 13	4.612	0.321	1.202	0.101	12.5	11.87	0.13	2.36	0.73	23.09	10.42	0.46	1.85	1.37	27.07	98.086
SWM 8 matrx mnz 14	1.698	0.267	0.377	0.084	12.5	11.87	0.13	2.36	0.73	23.09	10.42	0.46	1.85	1.37	27.07	94.276
SWM13 Mnz1 pt1	4.193	0.362	0.665	0.145	12.5	11.87	0.13	2.36	0.73	23.09	10.42	0.46	1.85	1.37	27.07	97.215
SWM13 Mnz1 pt2	3.091	0.246	0.597	0.133	12.5	11.87	0.13	2.36	0.73	23.09	10.42	0.46	1.85	1.37	27.07	95.917
SWM13 Mnz1 pt3	4.772	0.328	0.707	0.152	12.5	11.87	0.13	2.36	0.73	23.09	10.42	0.46	1.85	1.37	27.07	97.809
SWM13 Mnz4 pt1	2.77	0.341	0.706	0.119	12.5	11.87	0.13	2.36	0.73	23.09	10.42	0.46	1.85	1.37	27.07	95.786
SWM13 Mnz4 pt2	2.898	0.332	0.682	0.106	12.5	11.87	0.13	2.36	0.73	23.09	10.42	0.46	1.85	1.37	27.07	95.868
SWM13 Mnz4 pt3	3.232	0.357	0.713	0.111	12.5	11.87	0.13	2.36	0.73	23.09	10.42	0.46	1.85	1.37	27.07	96.263
SWM13 Mnz5 pt1	3.316	0.443	0.799	0.128	12.5	11.87	0.13	2.36	0.73	23.09	10.42	0.46	1.85	1.37	27.07	96.536
SWM13 Mnz5 pt2	2.416	0.348	0.62	0.106	12.5	11.87	0.13	2.36	0.73	23.09	10.42	0.46	1.85	1.37	27.07	95.34
SWM13 Mnz5 pt3	2.38	0.348	0.605	0.121	12.5	11.87	0.13	2.36	0.73	23.09	10.42	0.46	1.85	1.37	27.07	95.304
SWM6 Mnz1 pt1	3.027	0.287	0.085	0.065	12.5	11.87	0.13	2.36	0.73	23.09	10.42	0.46	1.85	1.37	27.07	94.397
SWM6 Mnz2 pt1	5.617	0.762	0.872	0.134	12.5	11.87	0.13	2.36	0.73	23.09	10.42	0.46	1.85	1.37	27.07	99.235
SWM6 Mnz3 pt1	3.576	0.287	0.076	0.076	12.5	11.87	0.13	2.36	0.73	23.09	10.42	0.46	1.85	1.37	27.07	96.612
SWM6 Mnz4 pt1	0	0	0	139.022	12.5	11.87	0.13	2.36	0.73	23.09	10.42	0.46	1.85	1.37	27.07	230.872
SWM6 Mnz5 pt1	6.108	0.055	0.304	0.103	12.5	11.87	0.13	2.36	0.73	23.09	10.42	0.46	1.85	1.37	27.07	91.914
SWM6 Mnz6 pt1	3.026	0.307	0.642	0.066	12.5	11.87	0.13	2.36	0.73	23.09	10.42	0.46	1.85	1.37	27.07	95.911
SWM6 Mnz7 pt1	3.928	0.581	0.796	0.097	12.5	11.87	0.13	2.36	0.73	23.09	10.42	0.46	1.85	1.37	27.07	97.076

SWM6 Mnz8 pt1	1.242	1.255	0.796	0.081	12.5	11.87	0.13	2.36	0.73	23.09	10.42	0.46	1.85	1.37	27.07	95.224
SWM6 Mnz9 pt1	4.145	0.351	0.865	0.089	12.5	11.87	0.13	2.36	0.73	23.09	10.42	0.46	1.85	1.37	27.07	97.3
SWM6 Mnz10 pt1	1.246	0.75	1.799	0.061	12.5	11.87	0.13	2.36	0.73	23.09	10.42	0.46	1.85	1.37	27.07	95.706
SWM6 Mnz11 pt1	2.764	0.044	0.796	0.071	12.5	11.87	0.13	2.36	0.73	23.09	10.42	0.46	1.85	1.37	27.07	95.525

Appendix II: X-Ray Maps

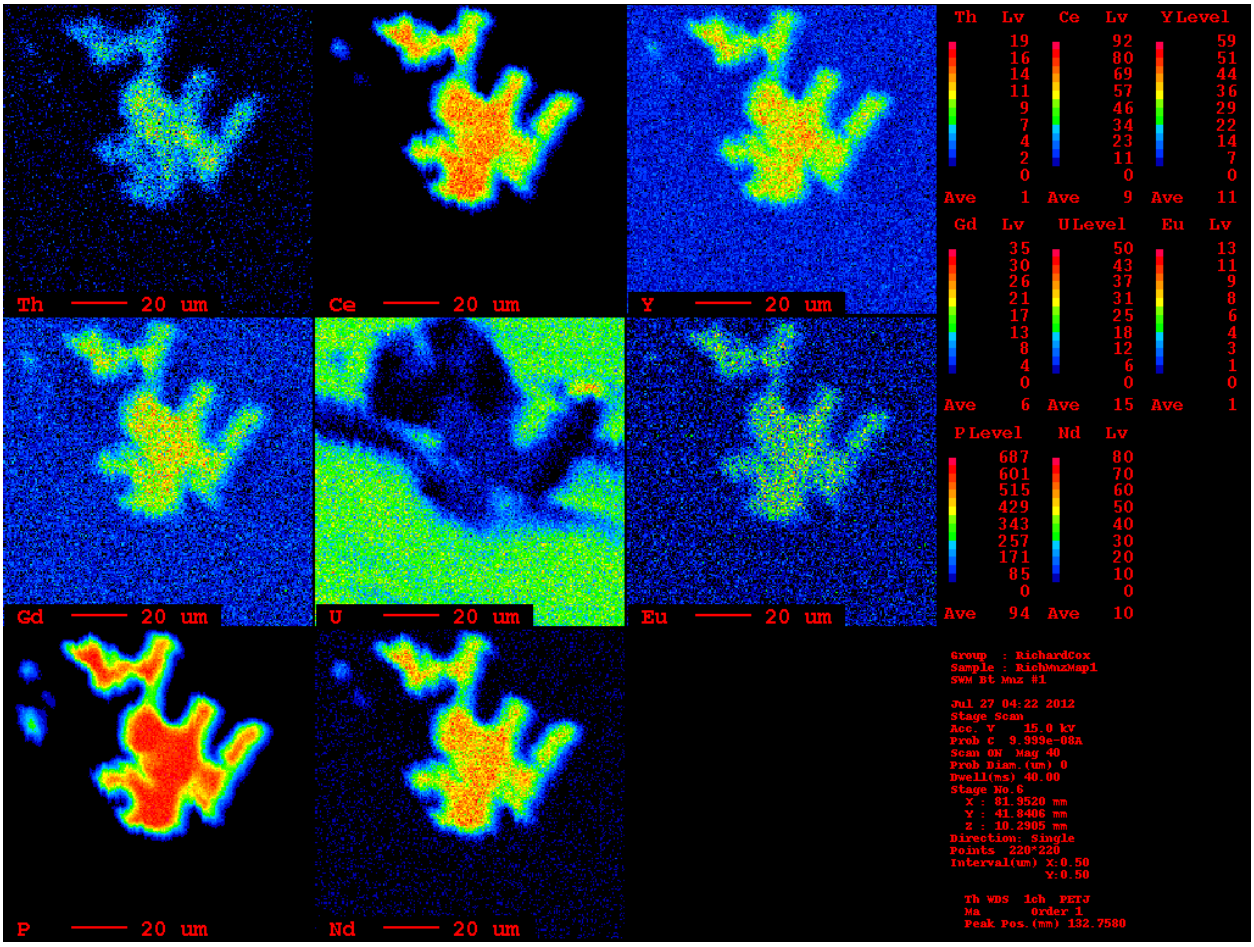

SWM-8 Bt Mnz1

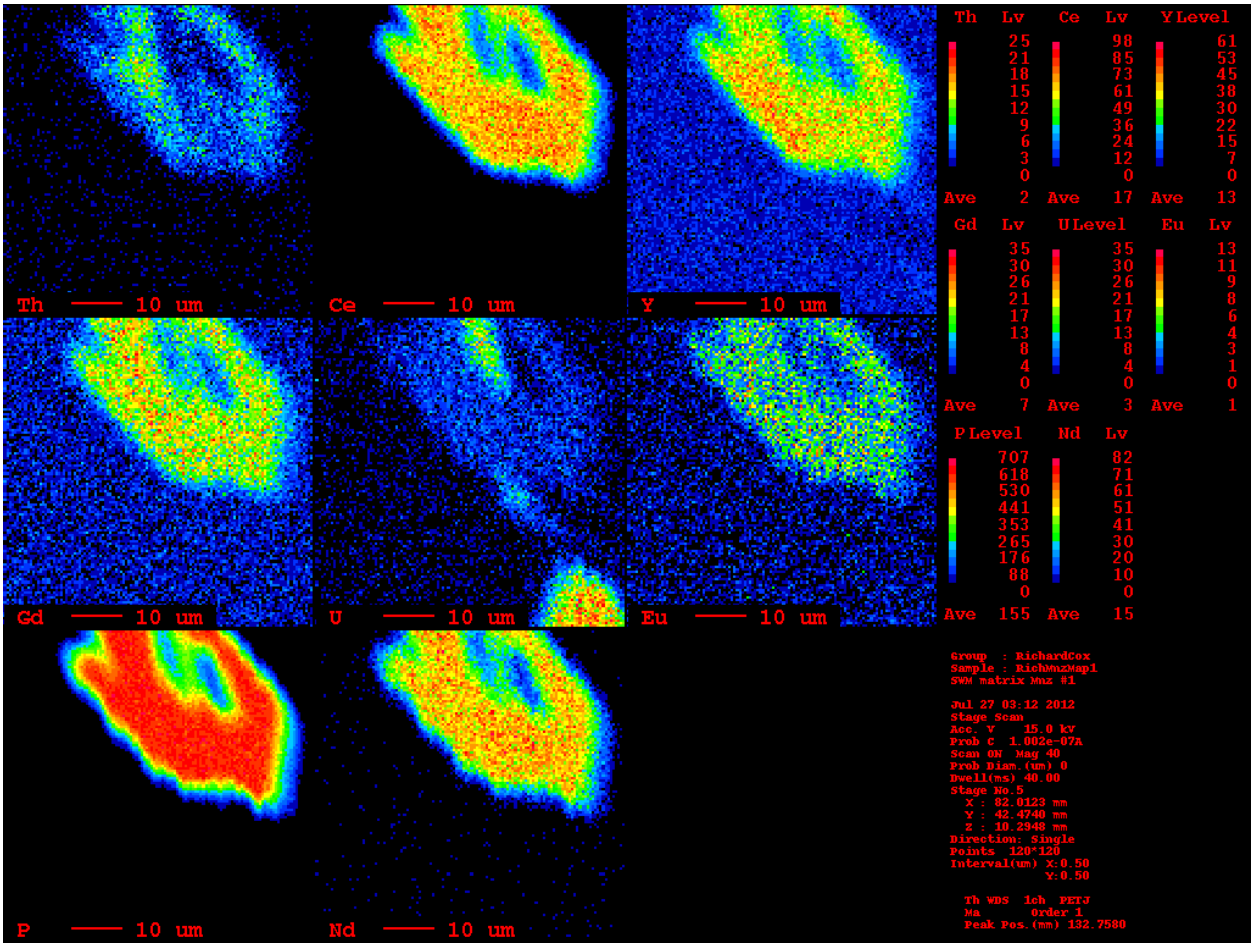

SWM-8 Mtx Mnz1

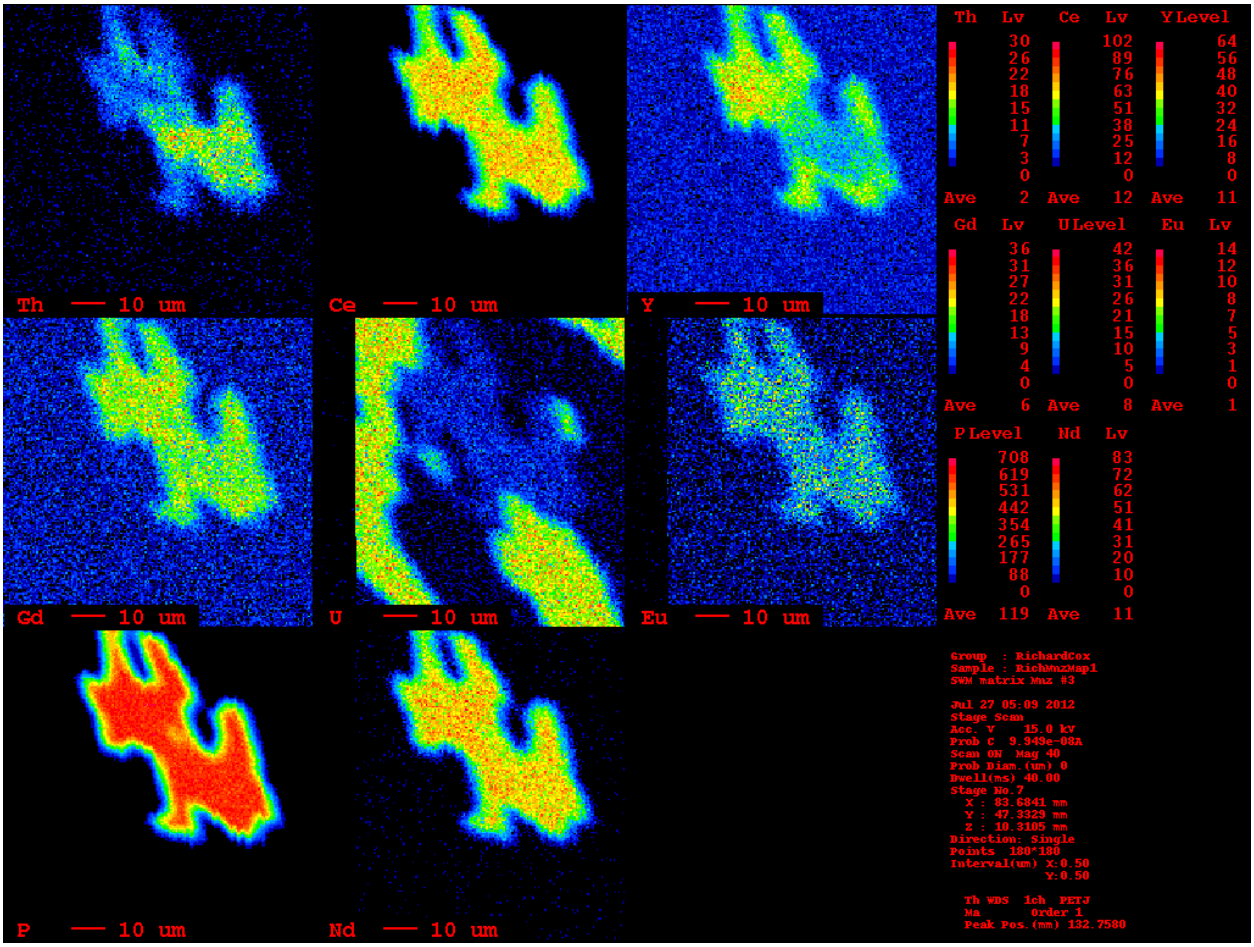
Th — 10 um
Ce — 10 um
Y — 10 um
Gd — 10 um
U — 10 um
Eu — 10 um
P — 10 um
Nd — 10 um
Th Lv
30
26
22
18
15
11
7
3
0
Ave 2
Ce Lv
102
89
76
63
51
38
25
12
0
Ave 12
Y Level
64
56
48
40
32
24
16
8
0
Ave 11
Gd Lv
36
31
27
22
18
13
9
4
0
Ave 6
U Level
42
36
31
26
21
15
10
5
0
Ave 8
Eu Lv
14
12
10
8
7
5
3
1
0
Ave 1
P Level
708
619
531
442
354
265
177
88
0
Ave 119
Nd Lv
83
72
62
51
41
31
20
10
0
Ave 11
Group : RichardCox
Sample : RichMnzMap1
SWM matrix Mnz #3
Jul 27 05:09 2012
Stage Scan
Acc. V 15.0 kv
Prob C 9.949e-08A
Scan ON Mag 40
Prob Diam.(um) 0
Dwell(ms) 40.00
Stage No.7
X : 83.6841 mm
Y : 47.3329 mm
Z : 10.3105 mm
Direction: Single
Points 180*180
Interval(um) X:0.50
Y:0.50
Th WDS 1ch PETJ
Ma Order 1
Peak Pos.(mm) 132.7580
SWM Mtx Mnz3

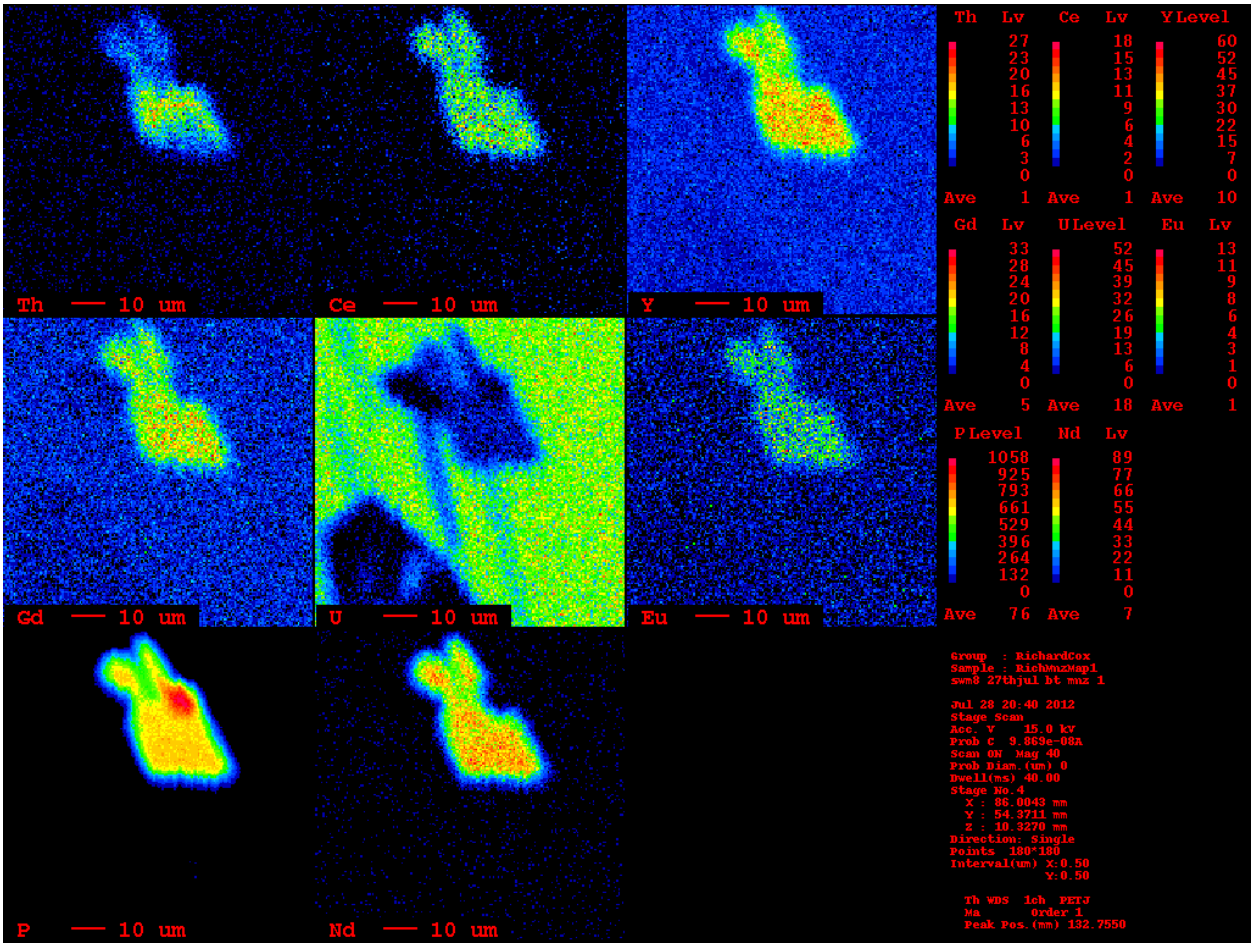

SWM-6 Mtx Mnz13

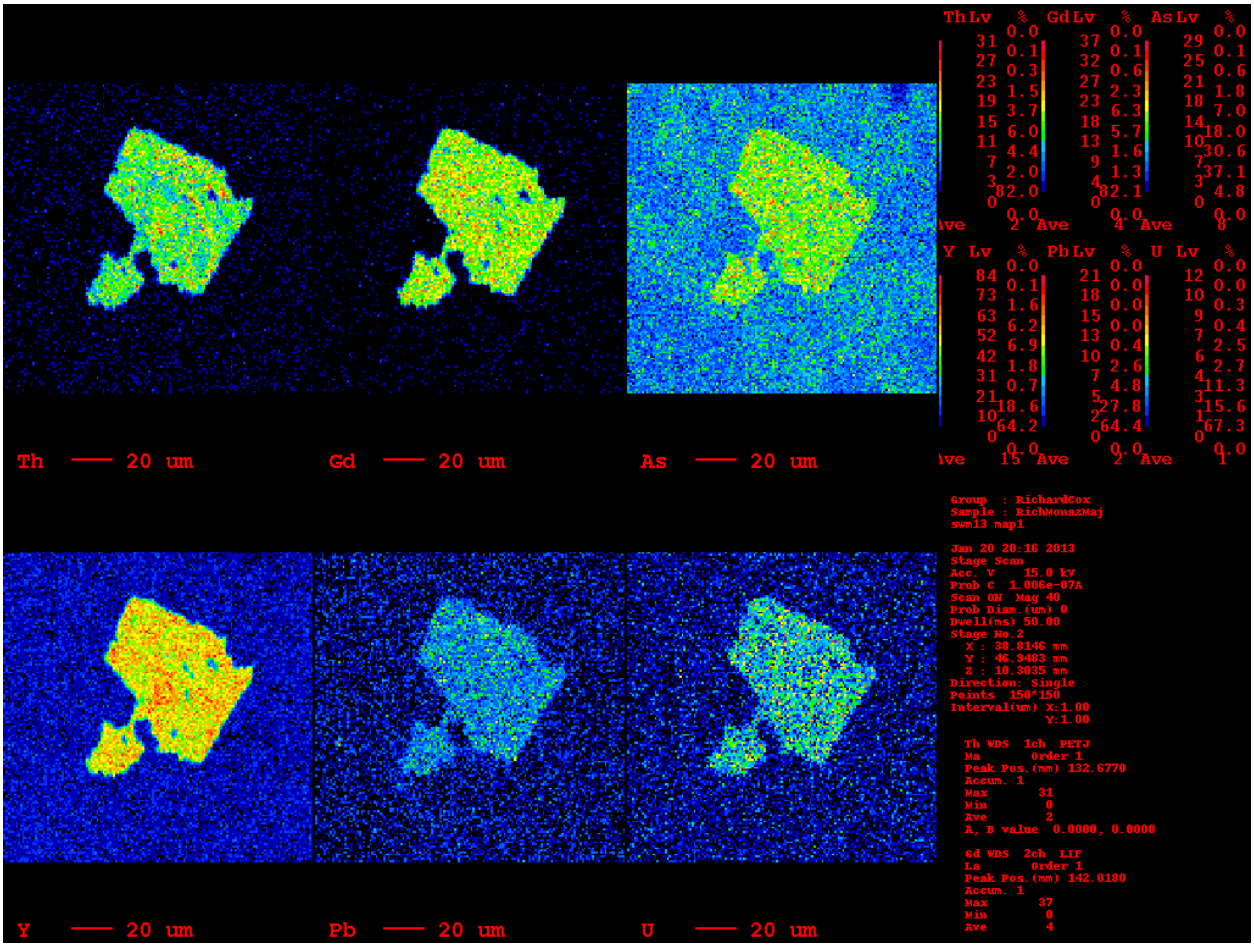

SWM-13 Mtx Mnz1

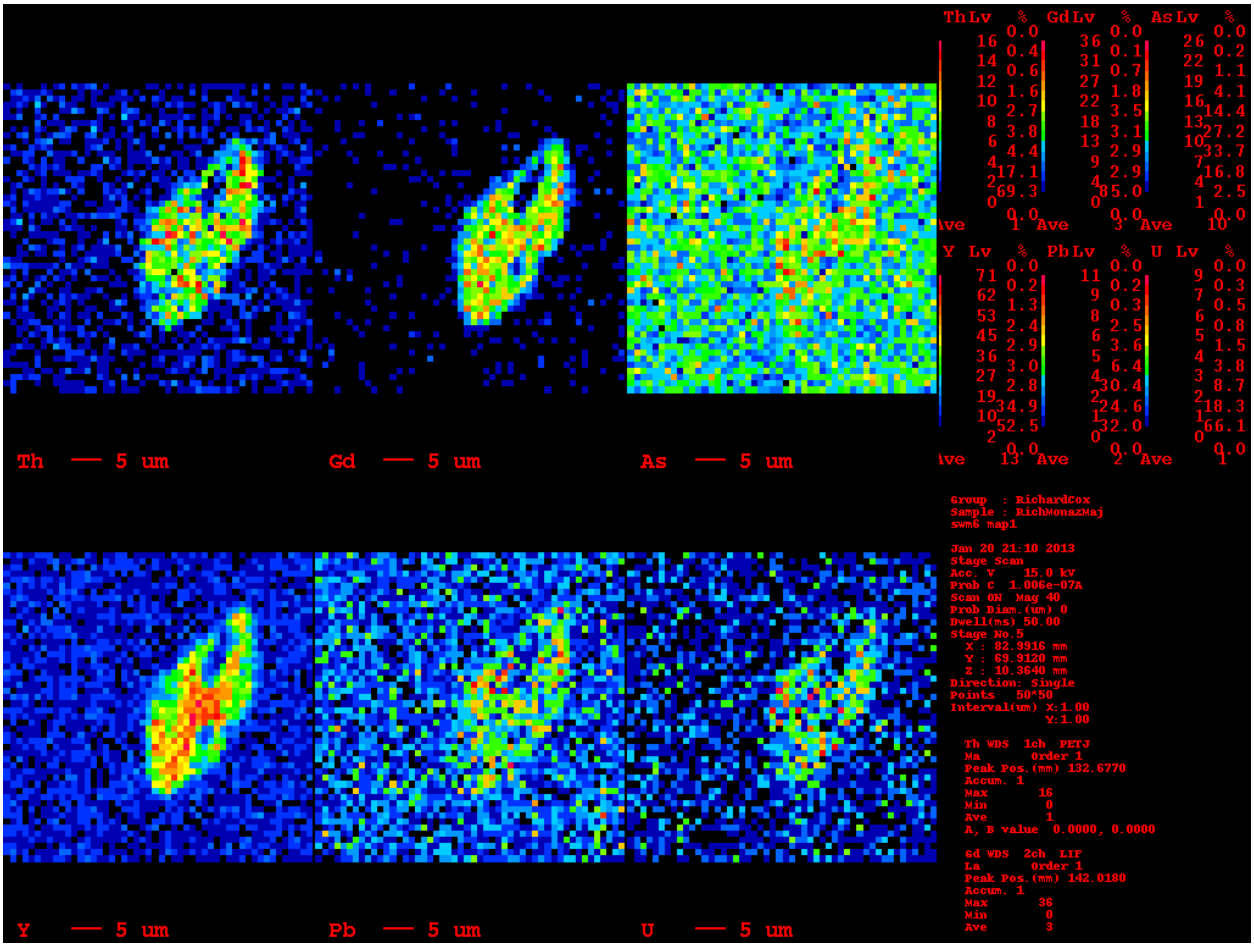

SWM-6 Mtx Mnz8

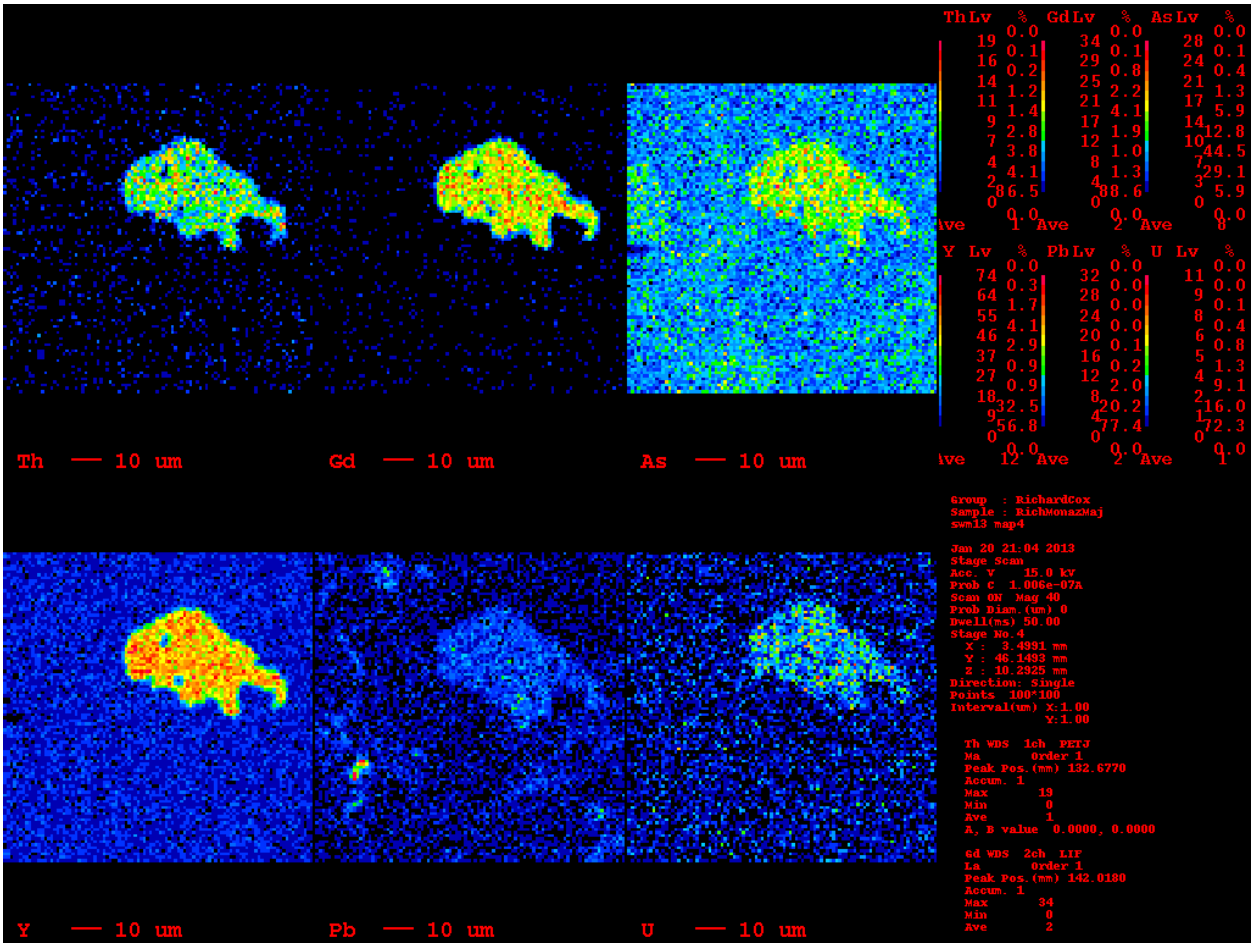

SWM-13 Mtx Mnz4

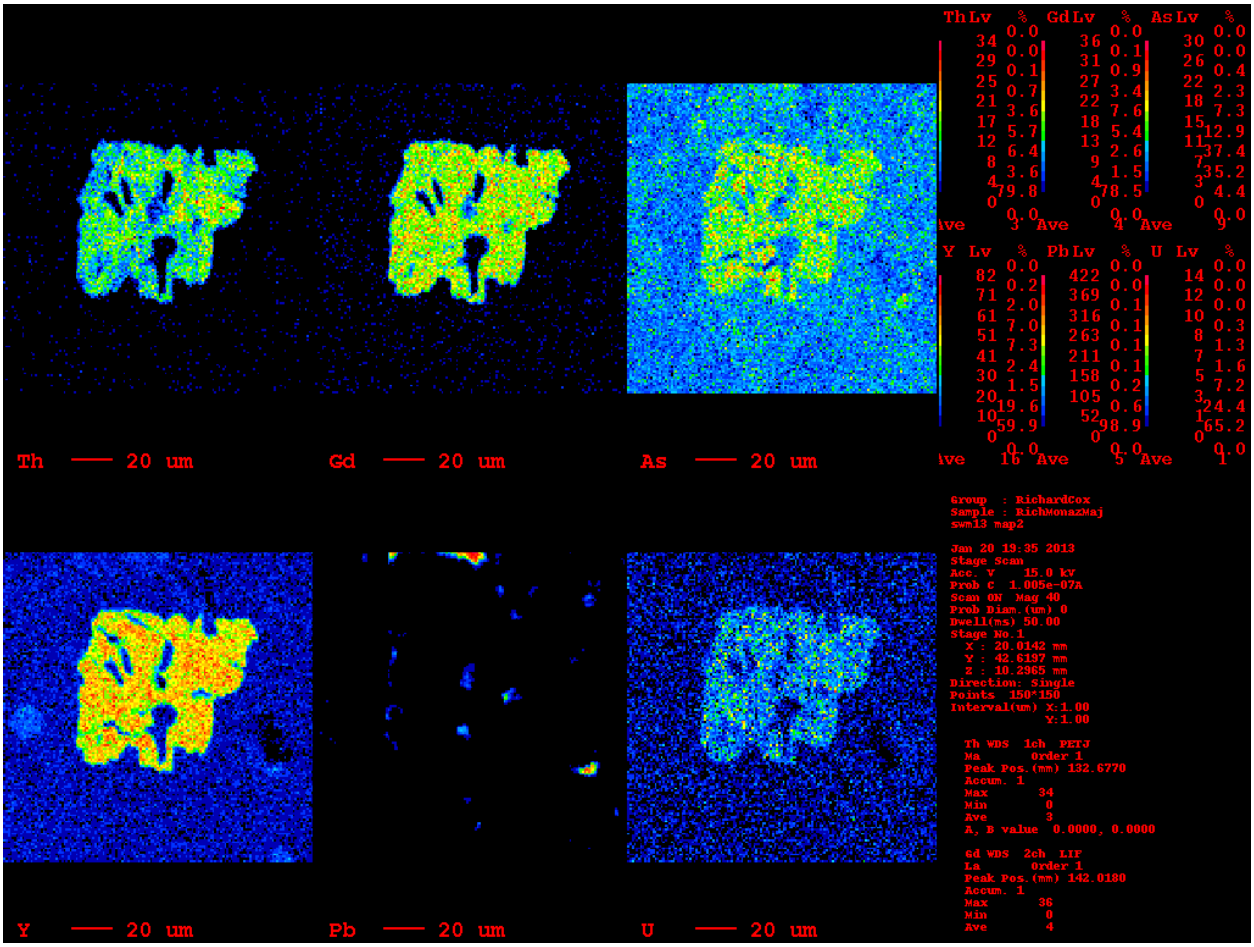

SWM-13Mtx Mnz2

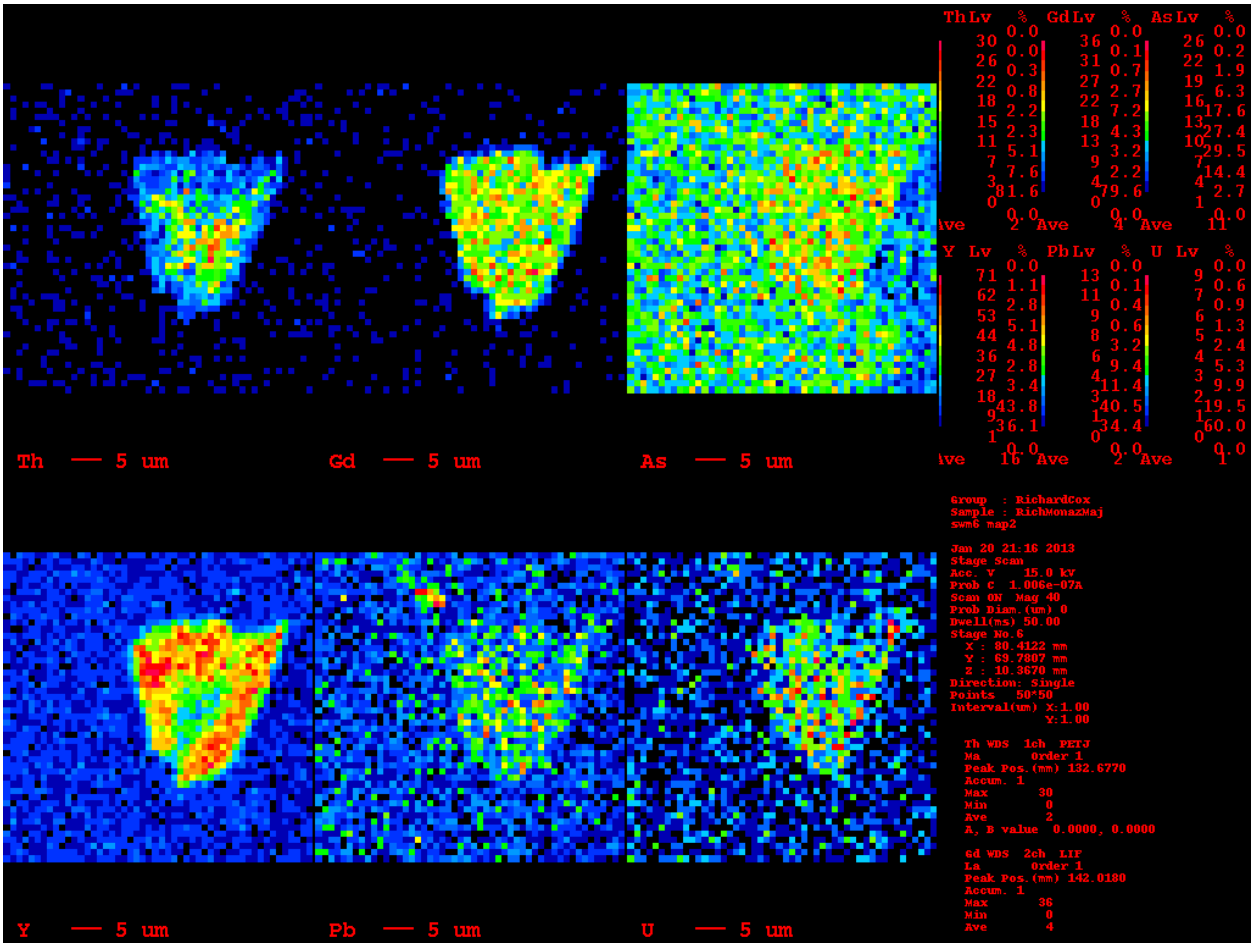

SWM-6 Mtx Mnz9

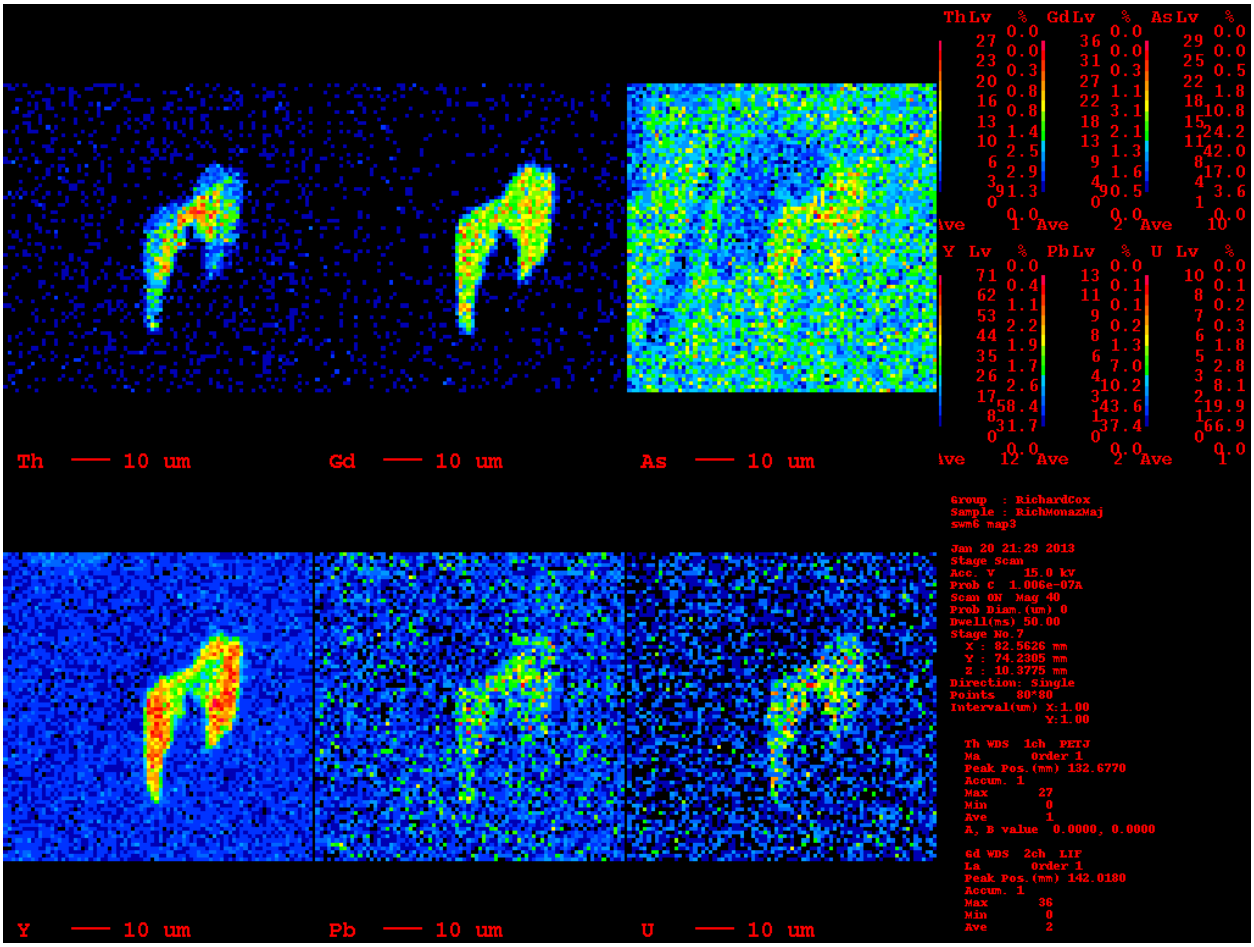

SWM-6 Mtx Mnz4

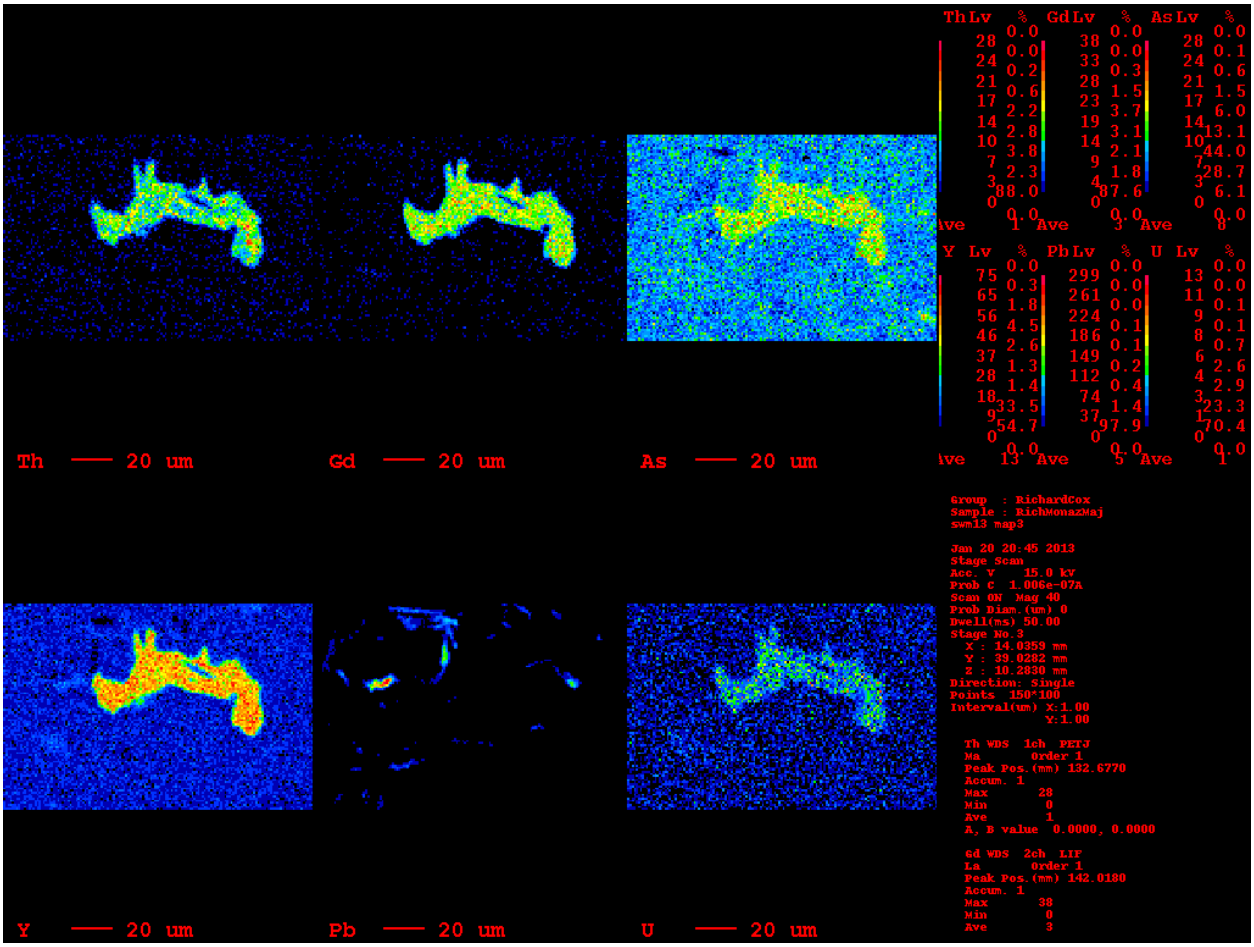

SWM-13 Mtx Mnz3